Câmara gama compacta para imagem médica em tempo real

João Marcos

LIBPhys - UC

Café com Física

16. Dez. 2020

Bem-vindos!

1290 UNIVERSIDADE D COIMBRA

Café com Física…

1 2 9 0 UNIVERSIDADE D COIMBRA

O **Café com Física** é um programa já com uns bons anos de emissão. Tem acompanhado várias gerações que passam e ficam ligadas ao Departamento de Física.

Uma persistência notável!

- Ocenano Pacífico: agora com **Marcos** André (após 28 anos com **João** Chaves), convidado há uns tempos do **Café da Manhã**, na celebração dos **35 anos de emissão** do programa
- Musica calma, alguns **clássicos**. Hoje, no Café com Física, falaremos de um equipamento que já pode ser considerado um clássico da imagiologia médica. Foi inventado na década de 50 (séc. XX).

Hal Anger (1922-2005)

Hal Anger presented in **1958** an equipment able to provide the positions of **γ-ray** interactions in a large-area position-sensitive detector, the **Gamma Camera**.

H. Anger was an american electrical engineer and biophysicist at Donner Laboratory, University of California, Berkeley

The Gamma camera is also called a **scintillation camera** or **Anger camera**

- Gamma cameras are used to perform **scintigraphy**: a medical imaging modality used to obtain functional images. E.g. cardiology, pneumology, oncology (staging of tumors, evaluate therapeutic response)

Heart study

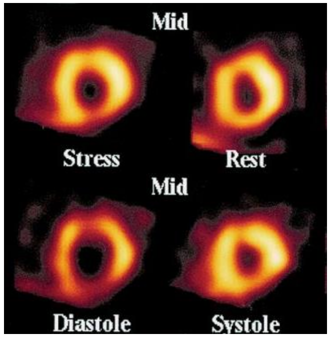

Bone scans

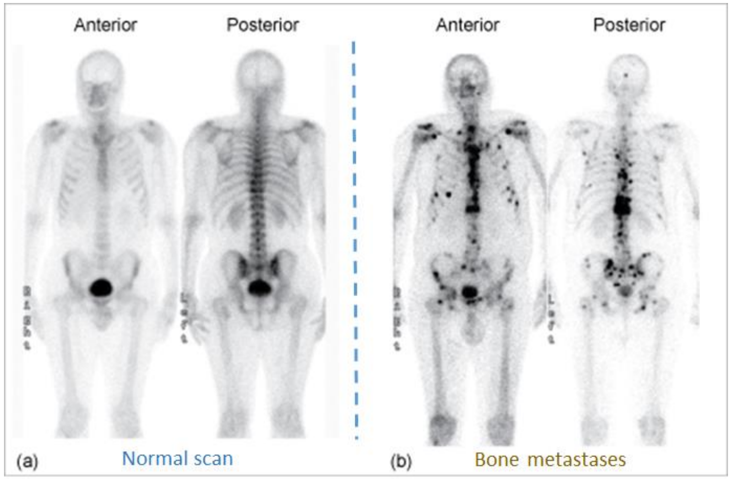

Lung scintigraphy

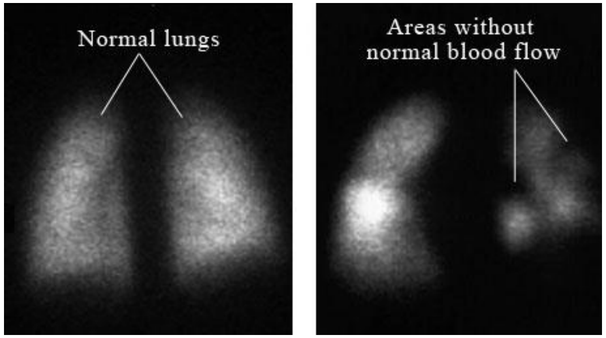

Kidneys study

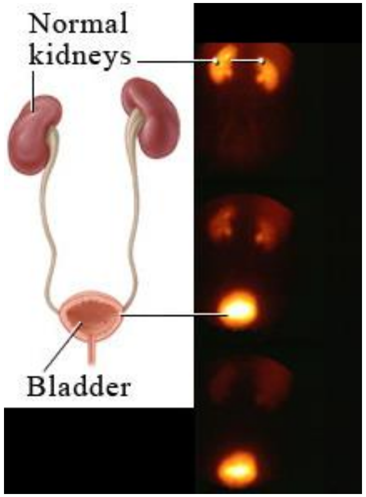

Gamma camera working principle

- For scintigraphy, the patient is injected with a **radiotracer** (radioisotope + biochemical substance) which **emits gamma-rays**
- Gamma camera obtains an image of the **projection** of the radiotracer through the collimator

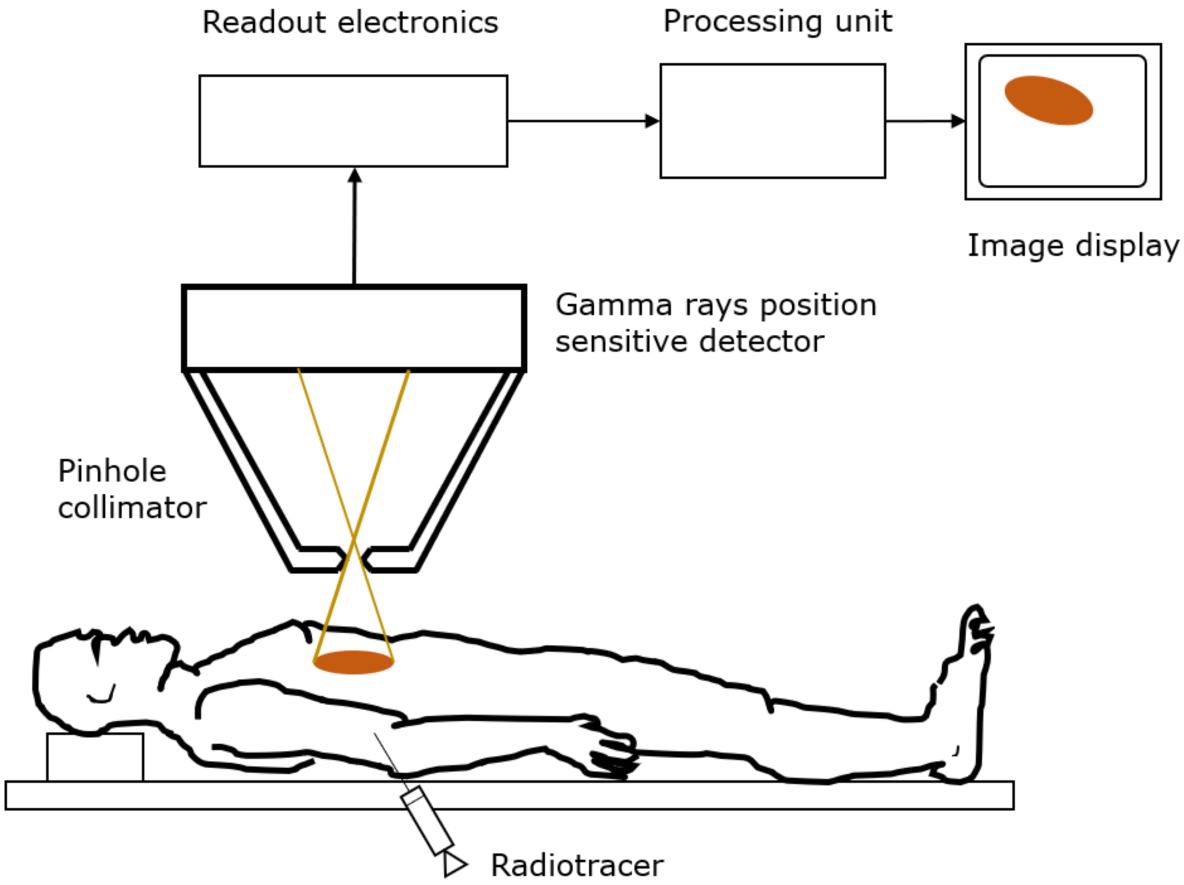

Gamma camera working principle

- For scintigraphy, the patient is injected with a **radiotracer** (radioisotope + biochemical substance) which **emits gamma-rays**
- Gamma camera obtains an image of the **projection** of the radiotracer through the collimator

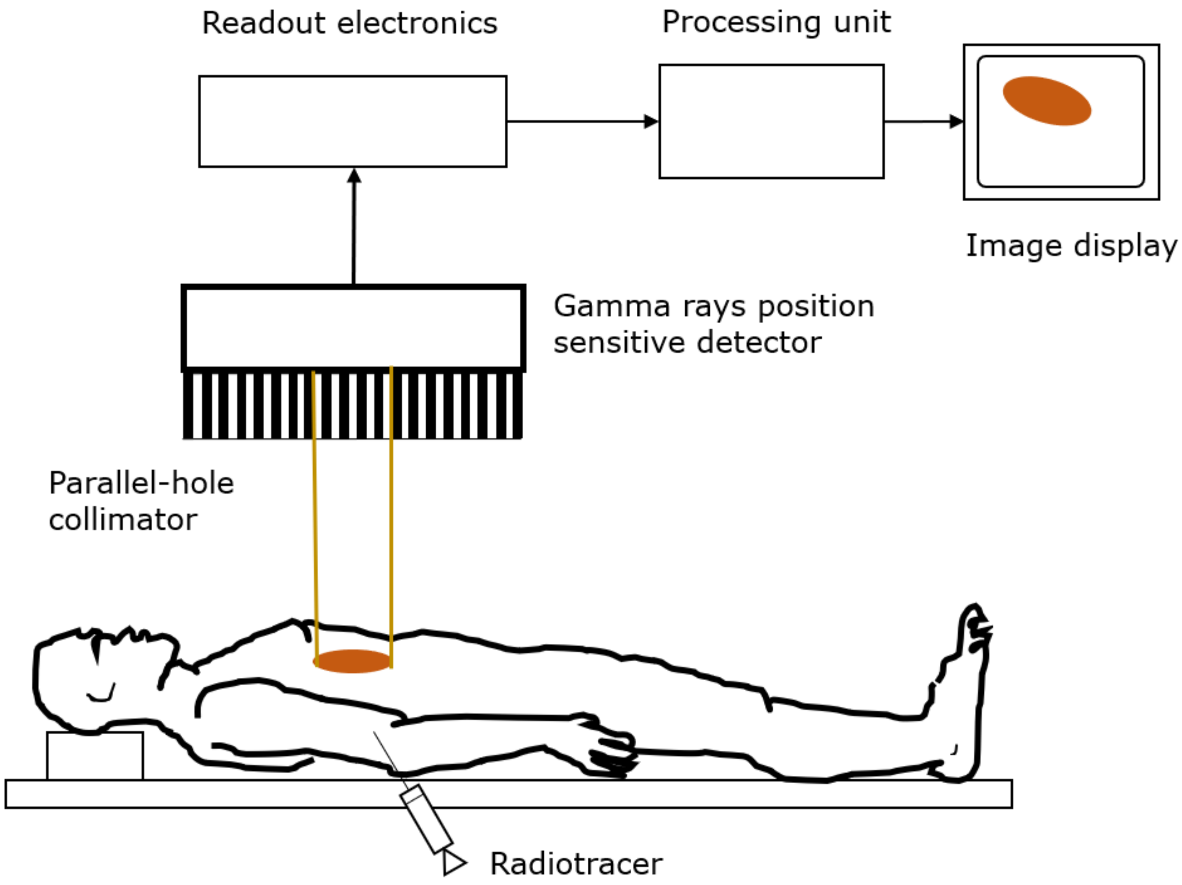

SPECT stands for "Single-photon emission computed tomography"

SPECT working principle

- The 3D dataset of γ-emitter distribution is obtained in SPECT by piling up many slices usually reconstructed independently

Gamma camera rotates around the patient to obtain several projection of the radiotracer inside the body

Recording of 1 projection of the radiotracer (scheme)

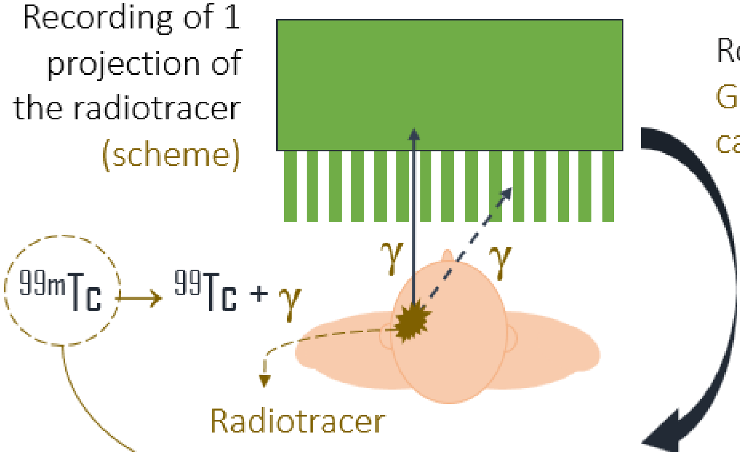

Radiotracer Inside the body

Rotating Gamma camera

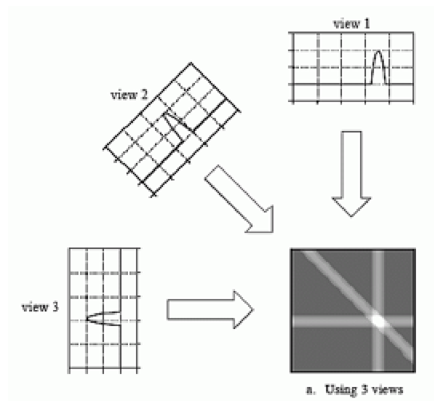

Projections at different angles

3D tracer distribution

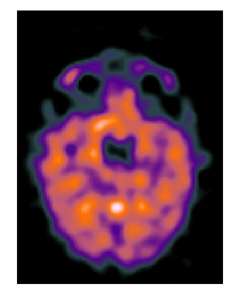

Brain example

Collaboration with Hospital (Coimbra)

- Collaboration with Universitary Hospital of Coimbra – Nuclear Medicine Department

THYROID:

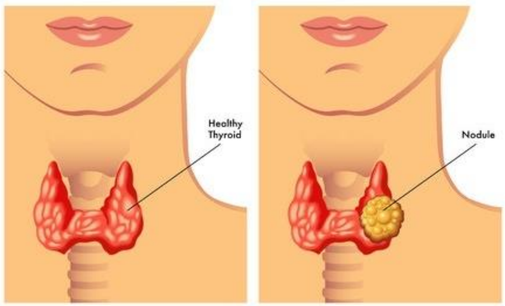

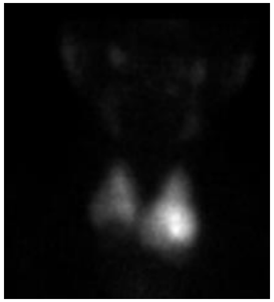

Thyroid scintigraphy with ^{99m}Tc showing a nodule of the left lower pole

SENTINEL LYMPH NODE BIOPSY (SLNB):

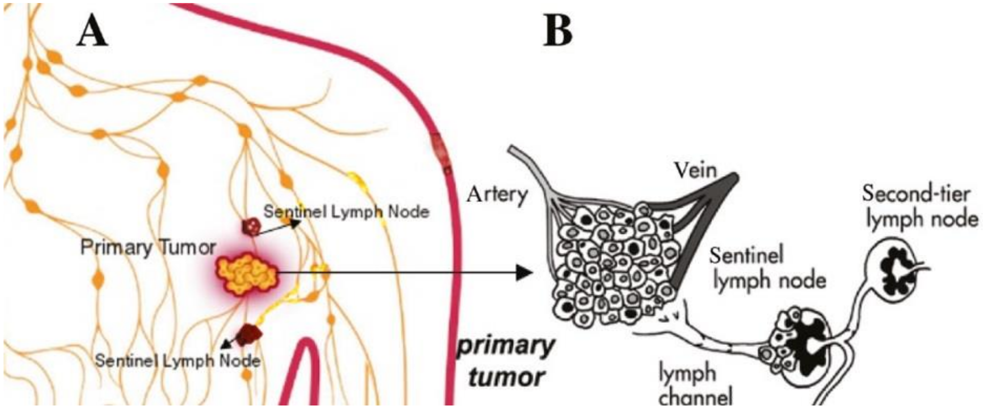

SLNB is used in melanoma and breast cancers staging

DOI: https://doi.org/10.1515/bmt-2016-0164

Lymphoscintigraphy

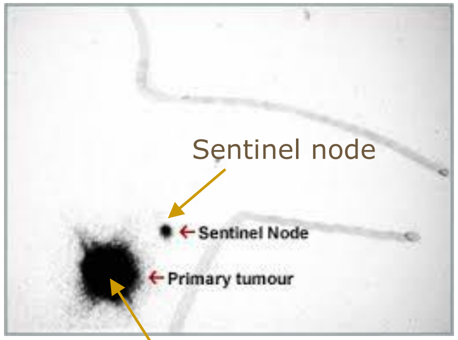

Injection site

Goal and requirements

GOAL: Real-time imaging system based on a **compact** gamma camera with **high-resolution**

Requirements of the gamma camera for SLN and thyroid imaging:

- Capable of real-time imaging
- Compact and Lightweight
- High extrinsic spatial resolution 5 mm at 5 cm
- Sub-millimetric intrinsic resolution
- Sensitivity: 100 cps/MBq
- Gamma ray energy: 140 keV
- Equipped with an interchangeable collimator: a parallel-hole and a pinhole collimator

Small field of view gamma cameras

Compact and lightweight devices appeared in the last 2 decades (commercial and research prototypes). They use different technologies.

Conventional (big) cameras

Compact gamma cameras

- Semiconductor based
- Scintillator based
  - Pixelated crystal
  - Monolithic crystal

Photosensors

- PSPMT
- SiPMs

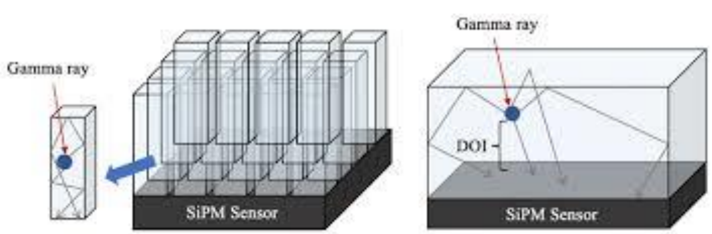

From Ting-Yi Yang thesis

64 channels
H12700B
(Hamamatsu)

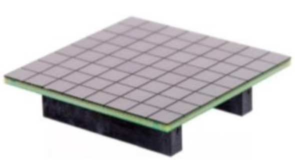

64 channels
G628-002MM
(SensL)

Examples of state-of-the-art compact gamma cameras

Name	Scintillator	Photosensor	Semiconductor	Size (mm^2)	Energy Res. (140 keV)	Spatial resolution (mm)	Collimator
Sentinella 102	Monolithic, CsI(Na)	PSPMTs	-	40x40	13%	9 @ 50 mm	Pinhole
Popovic	Monolithic, $LaBr_3$	SiPMs	-	60 mm Ø	21%	10.3 @ 50 mm	Parallel-hole
HiReSPECT	Pixelated, CsI(Tl)	PSMPTs	-	48x89	19%	3.5 @ 50 mm	Parallel-hole
GE (Haifa)	-	-	CdZnTe	40x40	8%	5 @ 50 mm	Parallel-hole
CrystalCam	-	-	CdZnTe	40x40	7%	5.4 @ 35 mm	Parallel-hole
eZScope	-	-	CdZnTe	32x32	9%	8 @ 50 mm	Parallel-hole
Tsuchimochi	-	-	CdTe	40x40	7.8%	6.3 @50 mm	Parallel-hole

Examples of state-of-the-art compact gamma cameras

Name	Scintillator	Photosensor	Semiconductor	Size (mm^2)	Energy Res. (140 keV)	Spatial resolution (mm)	Collimator
Sentinella 102	Monolithic, CsI(Na)	PSPMTs	-	40x40	13%	9 @ 50 mm	Pinhole
Popovic	Monolithic, $LaBr_3$	SiPMs	-	60 mm Ø	21%	10.3 @ 50 mm	Parallel-hole
HiReSPECT	Pixelated, CsI(Tl)	PSMPTs	-	48x89	19%	3.5 @ 50 mm	Parallel-hole
GE (Haifa)	-	-	CdZnTe	40x40	8%	5 @ 50 mm	Parallel-hole
CrystalCam	-	-	CdZnTe	40x40	7%	5.4 @ 35 mm	Parallel-hole
eZScope	-	-	CdZnTe	32x32	9%	8 @ 50 mm	Parallel-hole
Tsuchimochi	-	-	CdTe	40x40	7.8%	6.3 @50 mm	Parallel-hole

- The spatial resolution is mainly given by the collimator

Camera main components and features

- Based on the **experience of the group** it was decided to use a scintillator based camera, namely with:

  - **Monolithic** scintillator crystal
    - Allows to apply powerful methods for the reconstruction of scintillation events
    - To collect high amount of light (depending on the crystal light yield)

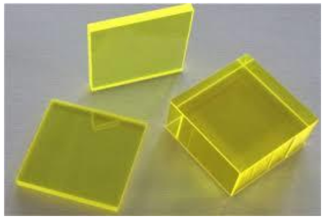

  - An array of **silicon photomultipliers** (SiPM)
    - Gain up to 10^6
    - Quantum efficiency up to 40%
    - Not sensitive to magnetic fields

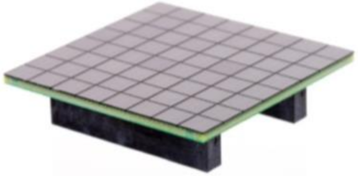

- Using an algorithm of the group might be possible to adapte automaticaly the camera response model in time (**self-calibration**). If so, it should be possible to **reduce the mantainance procedures**, reducing the camera downtimes. I have exploited this possility.

- **Objective:**

  To offer a state-of-the-art performance camera at a significantly lower price and which requires reduced mantainance procedures!

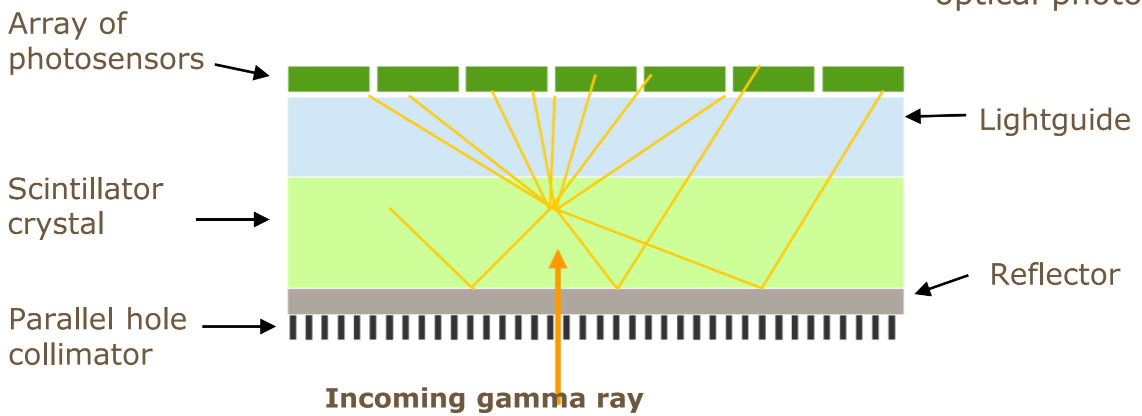

If the gamma ray deposit energy in the scintillator, optical photons are emitted isotropically

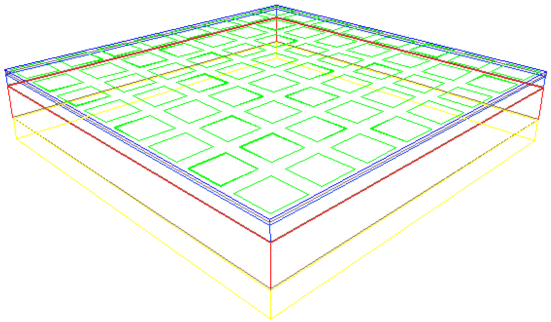

To obtain the *(x, y)* position of the scintillation events, the **mainstream method** of the available cameras is the centroid method:

$$x = \frac{\sum_i A_i x_i}{\sum_i A_i} \text{ and } y = \frac{\sum_i A_i y_i}{\sum_i A_i}$$

Centroid is robust, simple, but has three **significant drawbacks**:

- **Periodic calibrations are required**
- **Systematic spatial distortions**: look-up tables are used to correct the distortions
- **Limited capability to discriminate multiple events**: only by energy, which might fall within the total absorption peak

- I wanted to use **more advanced techniques** that permits to avoid the problems associated with CoG method and that can reduce maintenance

- The know-how of LIP on **statistical reconstruction methods** (e.g. dark matter search projects – LUX/Zepplin) were previously applied to medical gamma cameras by some colleagues

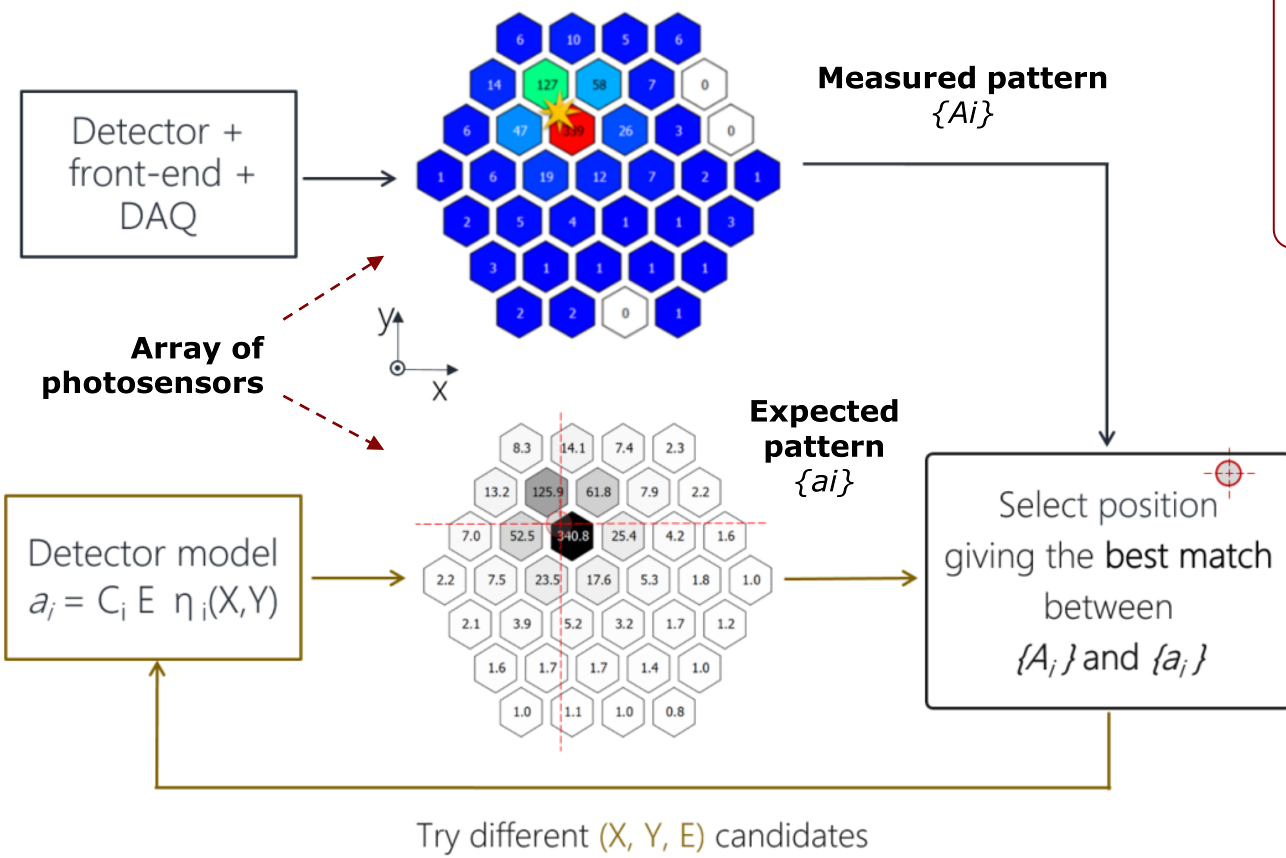

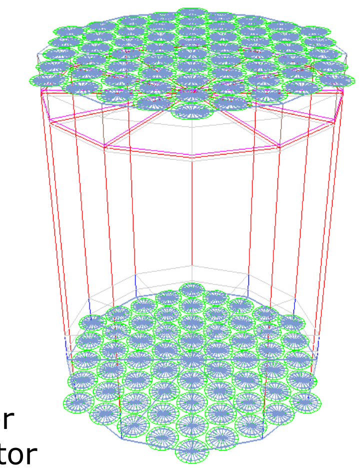

LUX – Dark matter detector

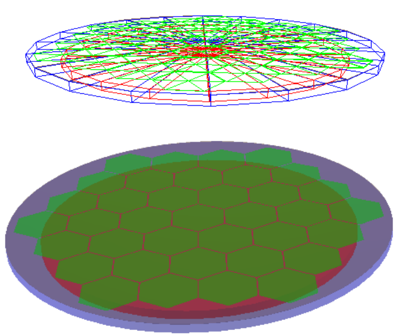

Medical gamma camera

Camera response model

- **Statistical reconstruction methods** require a **model** of the camera response to light

  Some **parametrization scheme** of the spatial response of the detector must be selected before building the model.

  The model is a set of **light response function (LRF)**, one per photosensor, as introduced in Zepplin project by Vladimir Solovov (LIP)

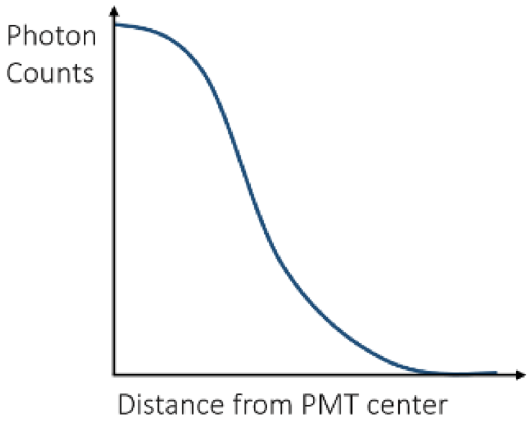

- **How to build the model?**

  Options

1. Register the photosensors signals for positions of scintillation events with energies within the photopeak – the position is assumed to be that of a pencil beam source moved along the entire camera field of view (experimental calibration)

2. Use data from simulation (signals vs source position)

3. Run a procedure that can **reconstruct automatically** the sensor responses to light from **food field** irradiation of the detector – I have exploited this approach

Adaptive algorithm for LRFs evaluation

Two sets of data are required as input for the LRF iterative reconstruction method:

- Vectors of measured photosensor signals – fixed during the iterative process.
- Estimated positions and energy (x, y, e) – updated at at each iteration.

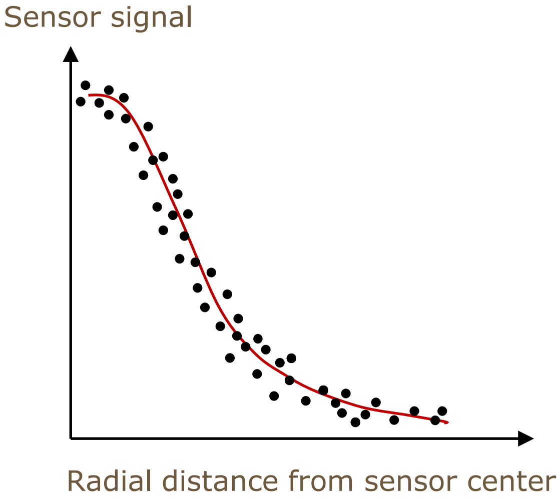

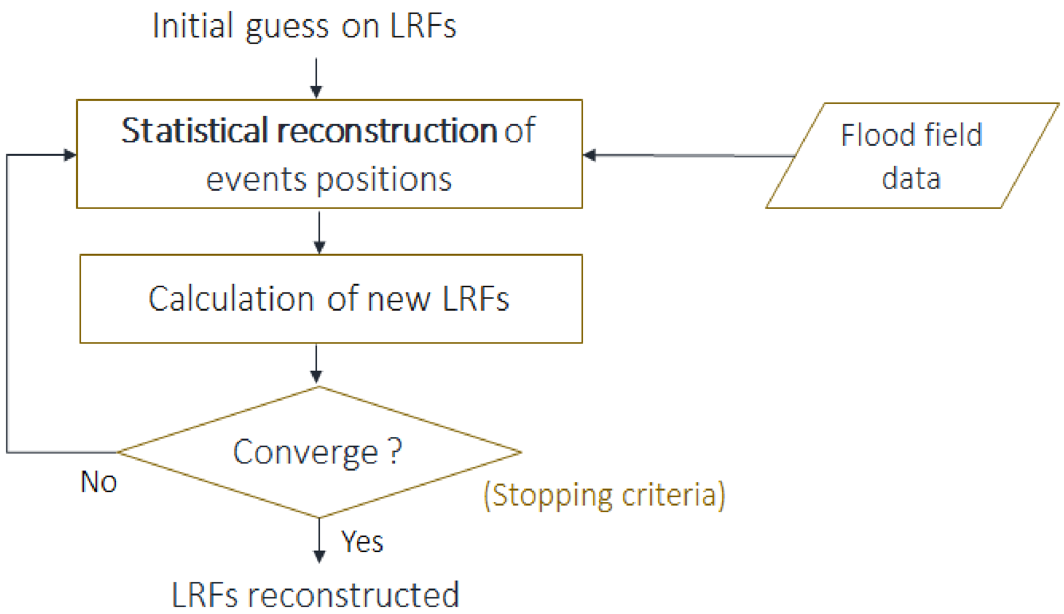

I have developed a **script for automatic execution of the interative procedure** to estimate the camera response model (LRFs)

Self-calibration of conventional camera

- The **iterative method** works very well with a conventional (**big**) camera, both in simulations and using a Retrofitted **clinical gamma camera** (Vladimir Solovov and Andrey Morozov work)

37 sensors (photomultiplier tubes)

Lightguide

NaI(TI)

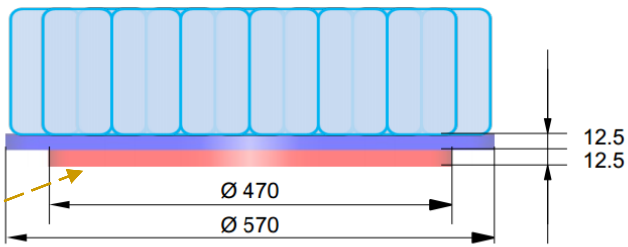

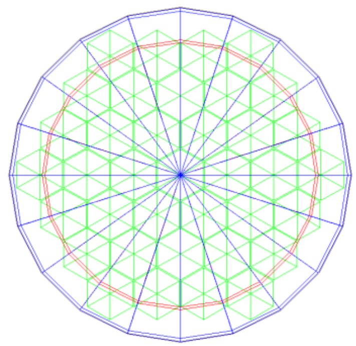

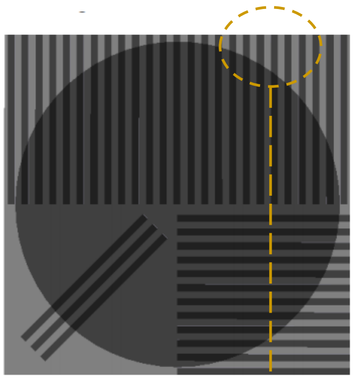

Phantom made of lead bars

Retrofitted **clinical gamma camera**

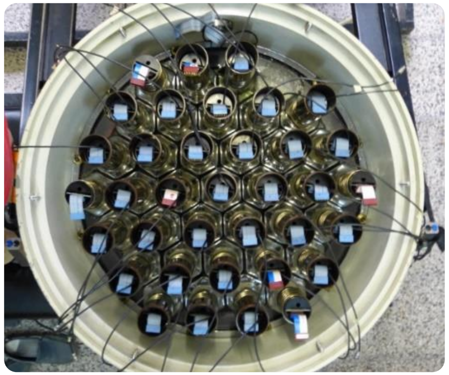

List mode readout

- The reconstruction results have many distortions using the initial guess on LRFs. The image quality improves using LRFs obtained in advanced iterations of the iterative method

Initial guess on LRFs: simulated LRF

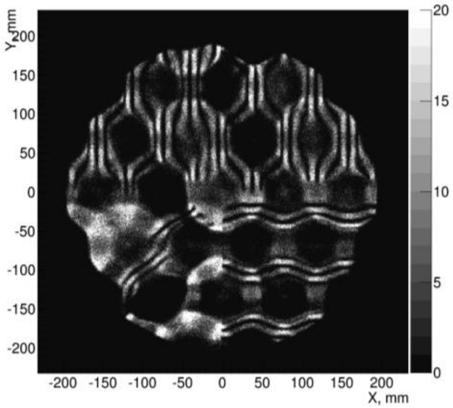

Phantom made of lead bars

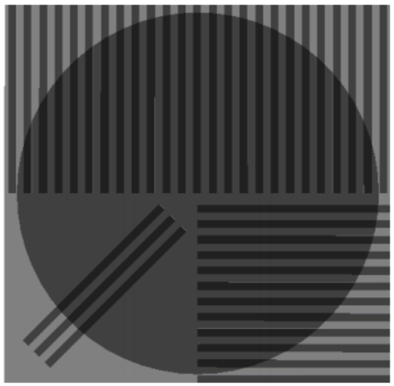

1st Iteration

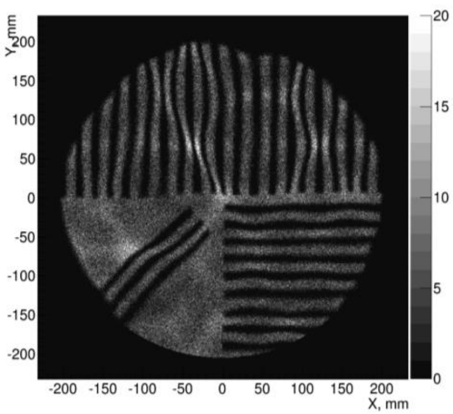

13th Iteration

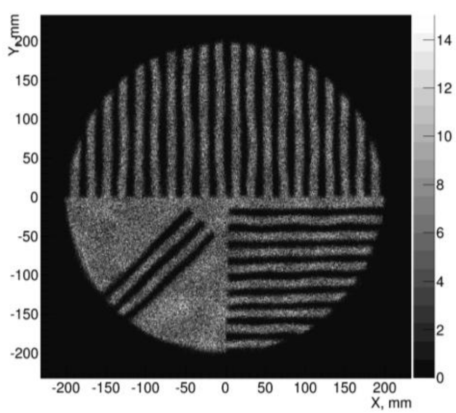

40th Iteration

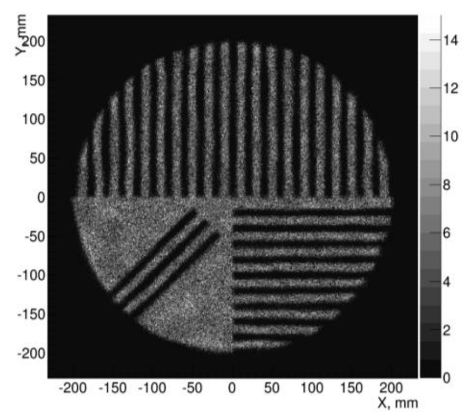

A. Morozov et al. 2015 Physics in Medicine and Biology, vol. 60, 4169

Design and optimization

1st objective: design and optimization of a compact gamma camera:

1) that respects the specified requirements

2) that is suitable for applying the adaptive method for LRFs reconstruction.

Method: Several rounds of Monte Carlo simulation *vs* experimental measurements (prototype)

Steps:

1) Create a camera model to be used in Monte Carlo simulation
2) Validate the **simulation models** by comparing with experimental data obtained from **prototypes**
3) Perform **optimization** of camera components

Camera parameters to optimize:

- **Crystal thickness**: efficiency *vs* spatial resolution
- **Lightguide thickness**: resolution *vs* distortions
- **Coupling compound** (low index *vs* high index compounds): the best resolution and the lowest degree of distortions

Camera optimization: ANTS2 and Geant4

- I made a model of the compact camera in **ANTS2** simulation package (LIP) for the tracing of the optical photons

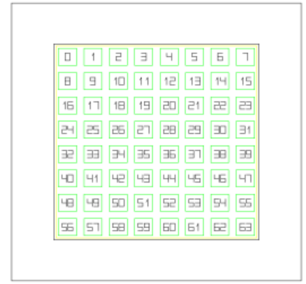

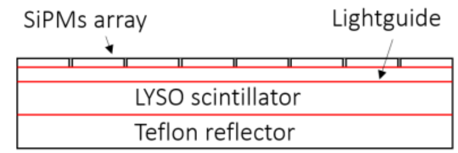

- During the **validation** against experimental results, I found some discrepancies and I have concluded that ANTS2 is not good enough for tracking gamma-rays

- In the group, Andrey Morozov have created a tool to **delegate the energy deposition** (tracking of gamma-rays) **to Geant4** (and send back the deposition positions to ANTS2)

Geant4 simulates three processes not present yet in ANTS2:

1) Coherent scattering
2) X-ray fuorescence and
3) Auger electron emission

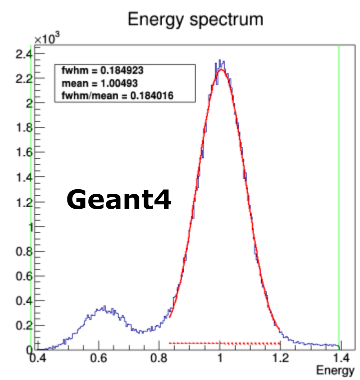

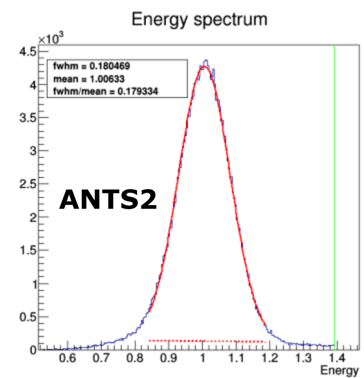

Comparison of energy deposition simulations in **ANTS2** and **Geant4**:

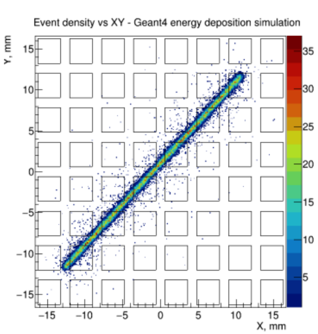

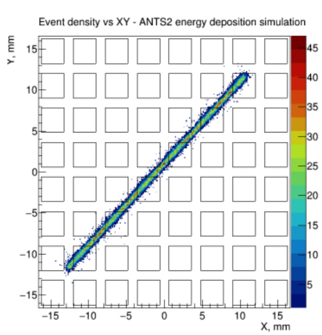

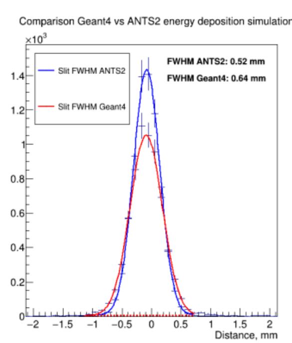

Geant4 results (spatial resolution) are closer to the experimental results than in ANTS2.

Optimization of camera prototypes

- I have started with **LYSO prototype** as the crystal is already available: **sufficient for thyroid**
- Due to **the intrinsic radioactivity of LYSO** (due to ^{176}Lu), for weak sources as in SLN imaging, the images obtained have low contrast
- I needed to find an **alternative material**: I proposed **GAGG** (when compared with LYSO, has: higher light yield and no self-radiation)

GAGG (3 mm thick) prototype

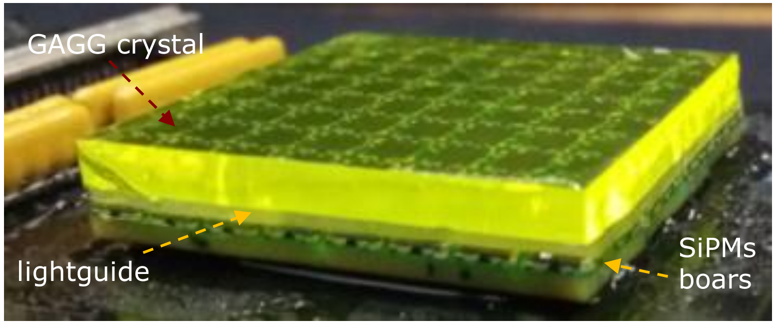

Ce:*GAGG*,
$Gd_3Al_2Ga_3O_{12}$:Ce

LYSO (2 mm thick) prototype

Ce:LYSO,
$Lu_{1.8}Y_{0.2}SiO_5$:Ce

Perspective view – reflector removed

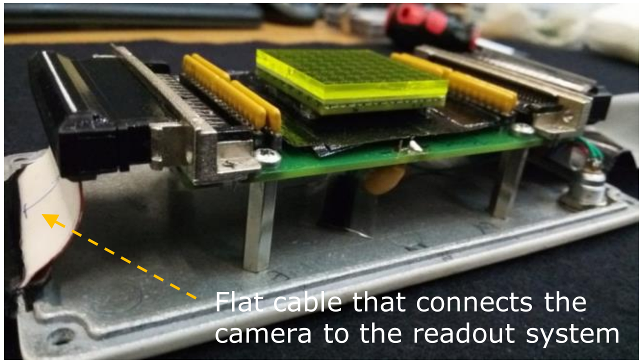

- **LYSO** has better efficiency and intrinsic resolution, however it is radioactive
- **GAGG**, with no self-radiation, is more suitable for SLN localization imaging

An array of **silicon photomultipliers** from SensL was used to collect the scintillation light

Array of photosensors selection

Analysis of the SiPMs PDE spectrum and scintillators emission spectrum

The **overlap** between the photon detection efficiency spectrum and the scintillator emission spectrum should be **maximized**

The effective PDE (PDE_{eff}) is the photon detection efficiency weighted by the crystal emission spectrum

The $\mathbf{PDE_{eff}}$ for LYSO is ~25% and for GAGG ~14% when
the SensL SiPMs working overvoltage is $\Delta V = 2.5$ V

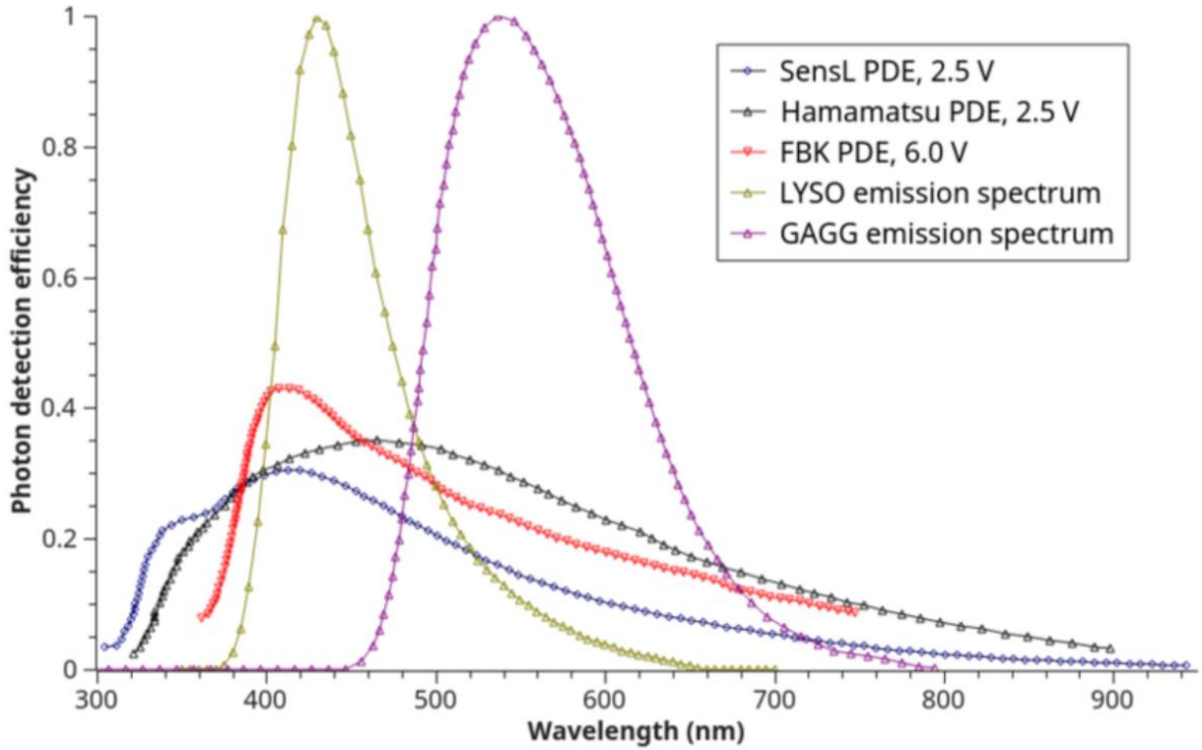

SensL Array-C, model 30035 was selected because it was offered for free to the Gamma Camera group by SensL company. Besides this, the SensL SiPMs have the lower dark count rate, a very important parameter.

Sir Isaac Newton: "Annus mirabilis"

Em Junho de **1665**, devido à grande peste de 1655 (só em Londes fez mais de 70.000 vítimas), a **Universidade de Cambrigde fechou portas.**

Newton acabado de se diplomar (com 23 anos) irá passar o ano na sua província natal (Lincolnshire, entre Londres e a Escócia), um ano rico em descobertas: o "**ano maravilhoso"**.

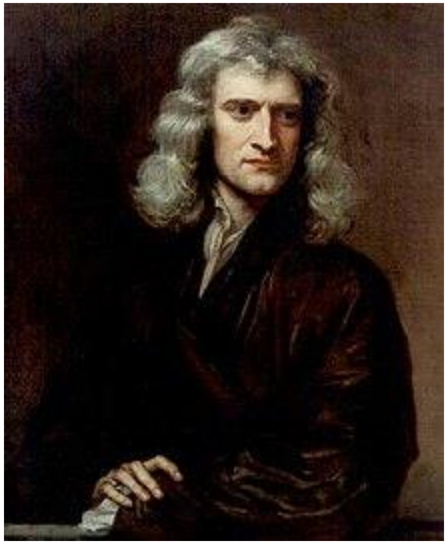

A partir de 1964 Newton anota as suas leituras. Sabemos que reflectiu sobre os Diálogos de Galileu, sobre a Geometria de Descartes e sobre os trabalhos de Kepler, em particular os que se referem à **luz e ao problema das cores**

Descobre que a luz "branca" é uma mistura de luz de todas as cores (e o prisma desvia-as em diferentes sentidos):

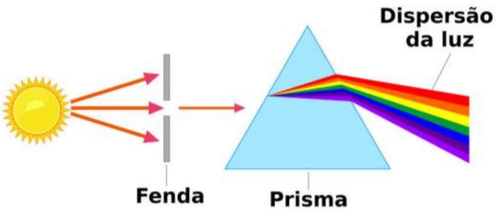

"… arranjei um prisma de vidro para realizar a célebre experiência das cores. Tendo para tal efeito obscurecido o meu quarto, e uma vez feito um buraquinho nas portadas para deixar entrar uma quantidade conveniente de raios de sol, coloquei o meu prisma encostado a esse burado, para refractar os raios na parede oposta. (…) foi muito agradável contemplar as cores vivas e intensas assim produzidas."

Mais à frente, com a ajuda de um furo numa prancheta, isola a parte azul (mais desviada pelo prisma) e **envia essa luz azul para um segundo prisma. Essa luz não se desdobra nem se tinge de outra cor!**

2nd objective: design and optimization of the collimators

Pinhole collimator

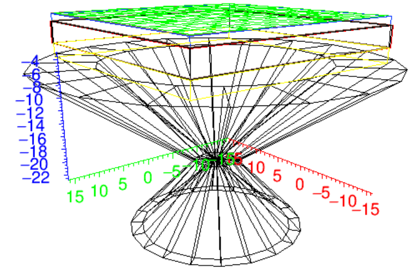

Previously: validation of the adequacy of the analytical equations available in literature for cameras of reduced sizes (simulations *vs* analytical results).

Target parameters:

Minimal requirements for **SLN imaging** also suitable for **thyroid**:

- Spatial resolution: < **5 mm at 5 cm**
- Efficiency: > 0.0001 **(100 cps/Mbq)**

Parallel-hole collimator

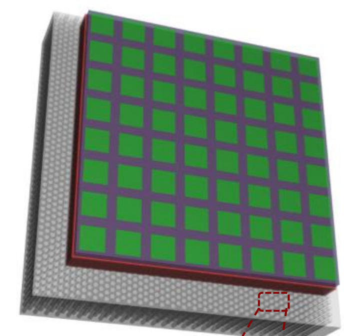

Ex: Parallel-hole collimator **trade-off curves:**

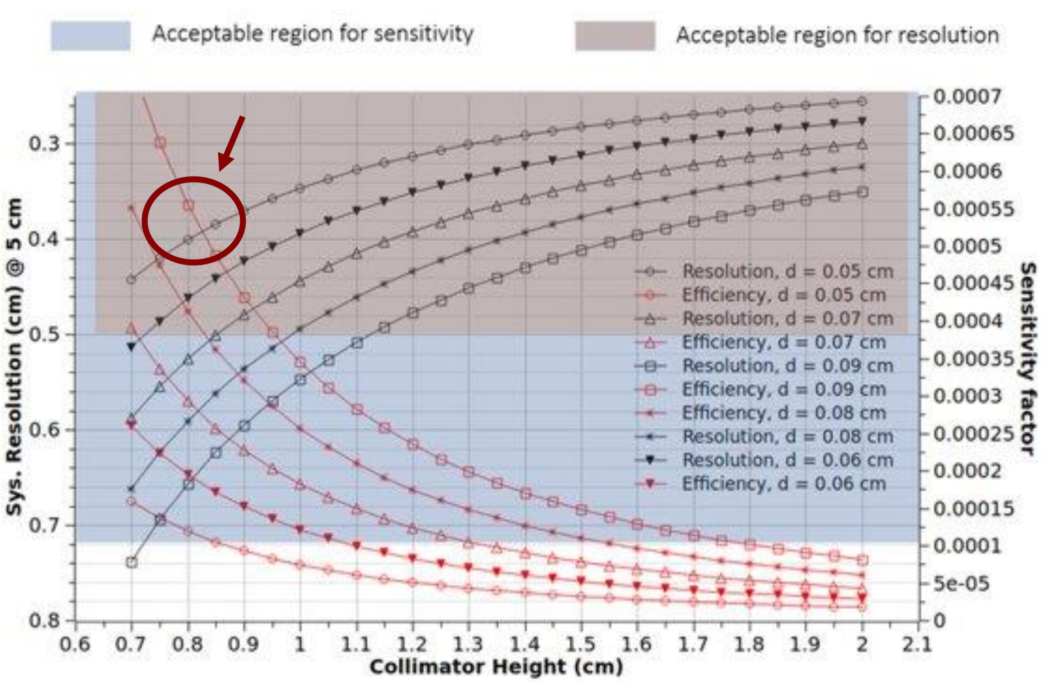

Parallel-hole collimator optimized parameters:

d = 0.05 cm
septa t = 0.03 cm
height = 0.8 cm

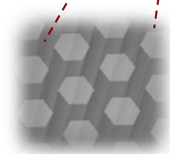

Spatial resolution: **4.1 mm (at 5 cm)**
Sensitivity**: 120 cps/MBq**

Collimator prototypes

Collimators are commonly made of **lead** (toxic). **Tungsten** can be used instead (shorter attenuation lenght than lead, which allows to use less material)

I have designed and ordered two collimators.

- **Parallel-hole collimator** (hexagones with 0.5 mm "diameter" *d*, septa *t* of 0.3 mm):

CAD design: Engº Rui Alves (LIP workshop)
Manufacturer: M&I Materials (UK)

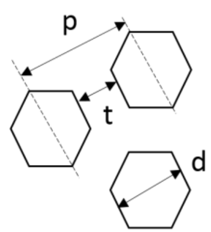

p = 0.8 mm
d = 0.5 mm
t = 0.3 mm

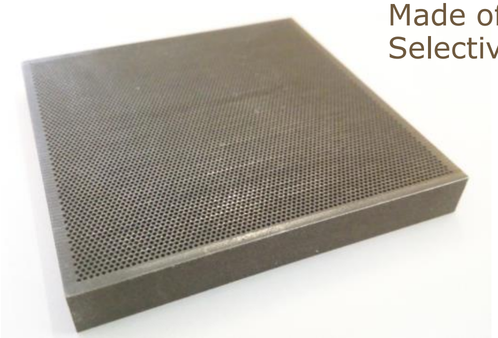

Made of **tungsten** using Selective laser melting (SLM)

Holes area:
60 x 60 mm²

Thickness (height):
8 mm

- **Pinhole collimator** (1 mm diameter hole and 0.5 mm channel height):

CAD design and manufacturing: DURIT (Albergaria-a-Velha)

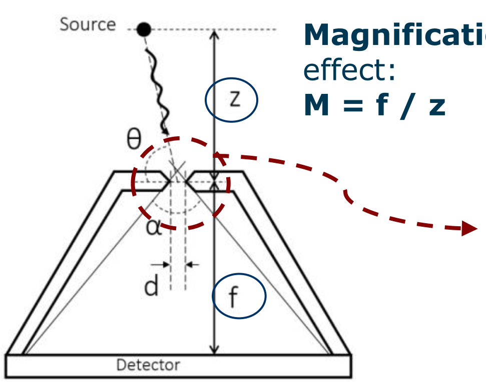

Magnification effect:
M = f / z

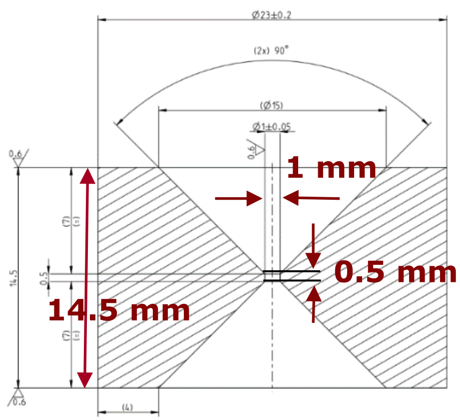

Made of **tungsten alloy** (95.5% W, 4.5% Co) using Electric discharge machining (EDM)

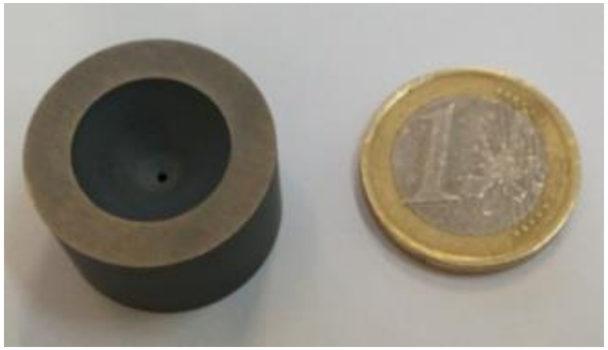

Readout and acquisition system

Selected readout: TRB3 (GSI) based readout for 64 channels

Acquisition rate up to 10 kHz

Signal waveform

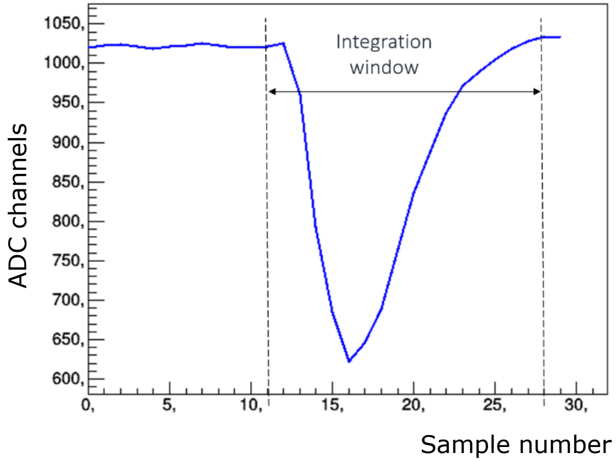

ADC channels per photoelectron

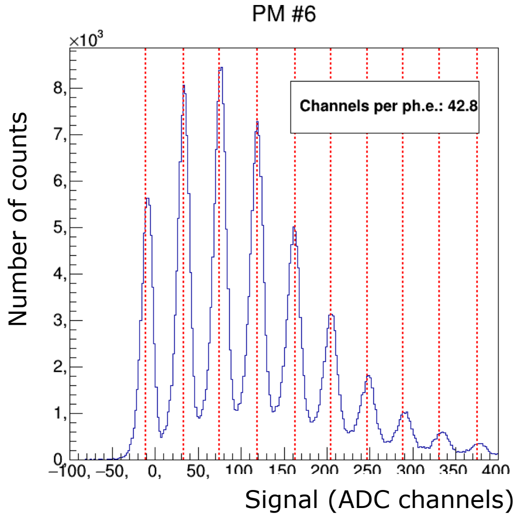

Example of a **scintillation event**:

64 SiPM Signal waveform

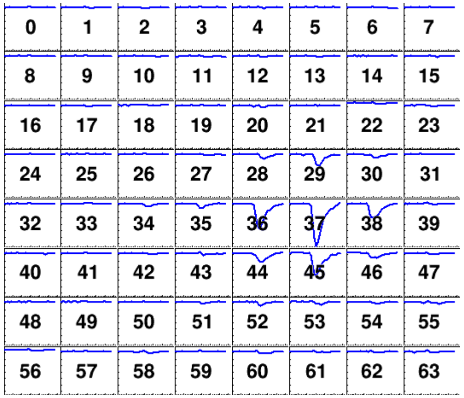

Number of detected photons

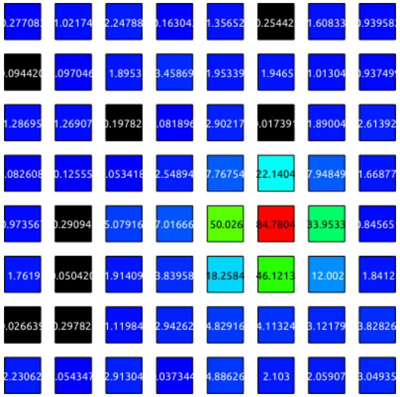

Real-time workflow

Real-time imaging has some challenges: acquisition rate, processing speed (waveforms, reconstruction algorithm)

The **scripts** required to extract waveform samples sent from the DAQ and the consecutive processing chain until the visualization of the event positions were prepared

- **For real-time** processing, a loop waits for waveform files and triggers their processing:

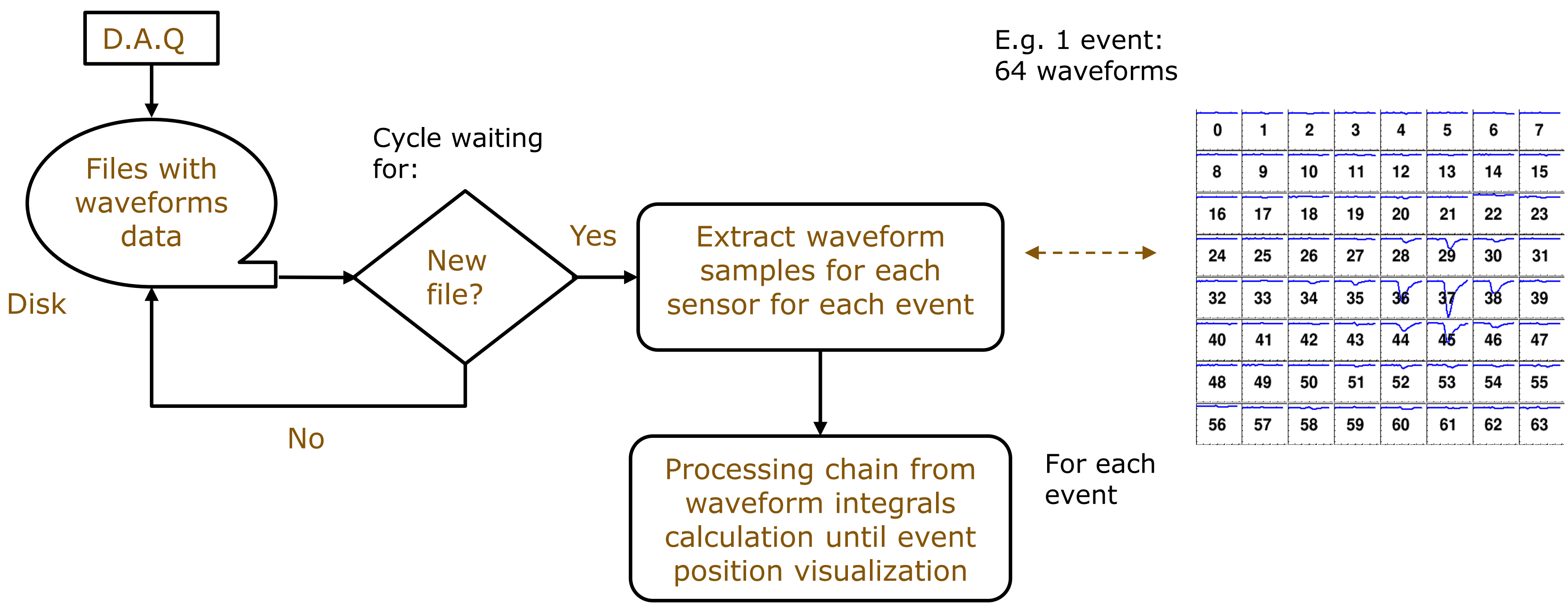

UNIVERSIDADE D COIMBRA

For each event in the file:

1 Calculation of signal **integrals**

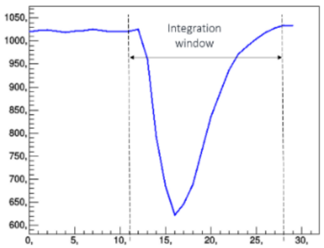

2 **Conversion** into number of photons

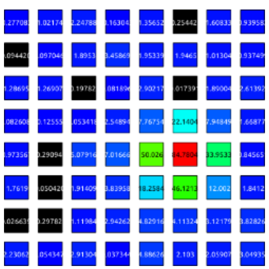

3 Apply **event reconstruction** (statistical algorithms): XY positions and energy

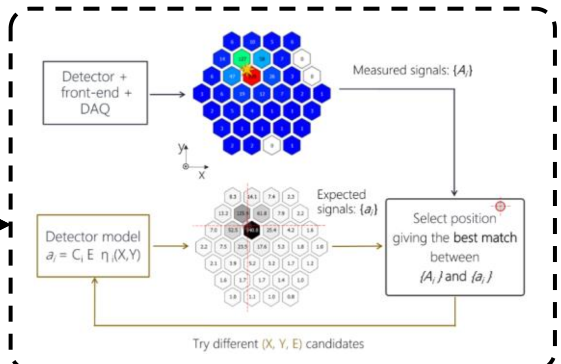

4 **Visualization** of the reconstructed XY event positions in a density plot

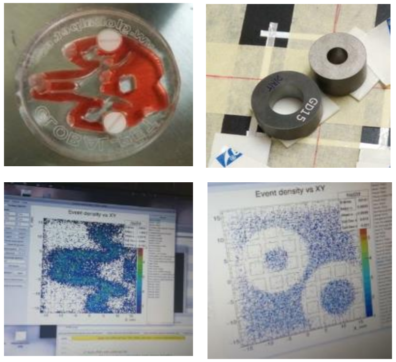

Real-time buffer (FIFO)

Save event signals (in number of photons) and reconstructed XY positions

Prototypes characterization

- The prototypes assessment was performed in the Universitary hospital of Coimbra (CHUC), with access to high activity source (^{99m}Tc, 140 keV)

Schematic drawing parallel-hole + gamma camera:

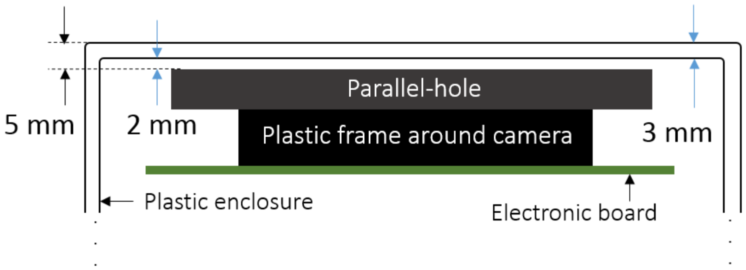

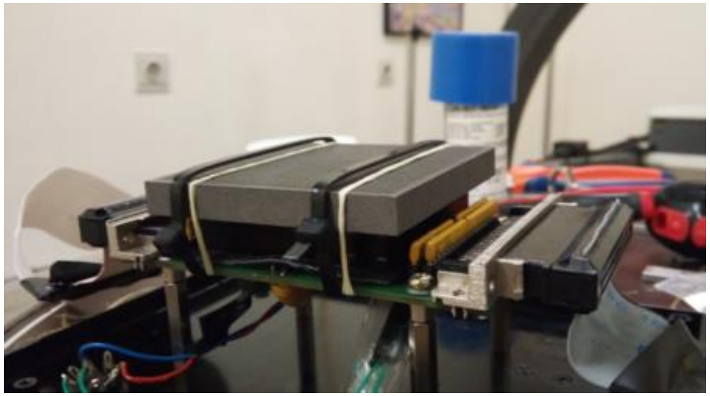

Storage (computer)

Controller mini-PC (hidden)

Readout system box

Compact gamma camera

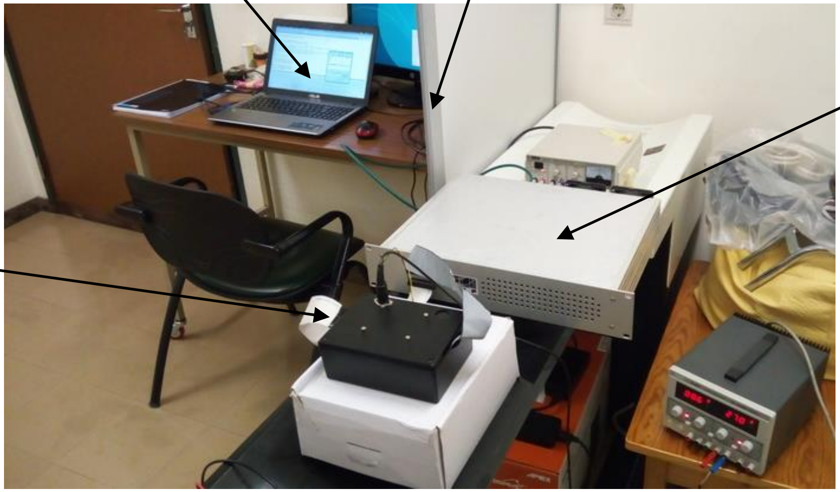

Masks and phantoms

Source position

Masks:

Parallel bars 2 mm wide

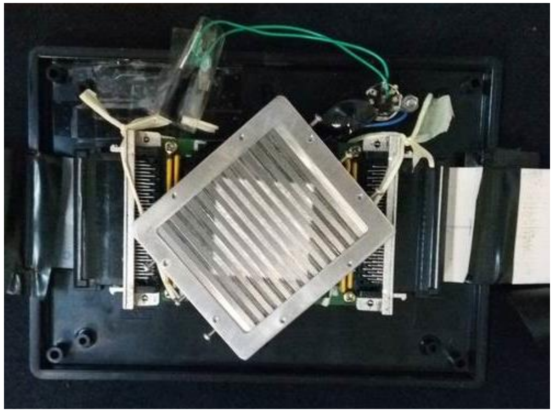

Four parallel 0.2 mm slits

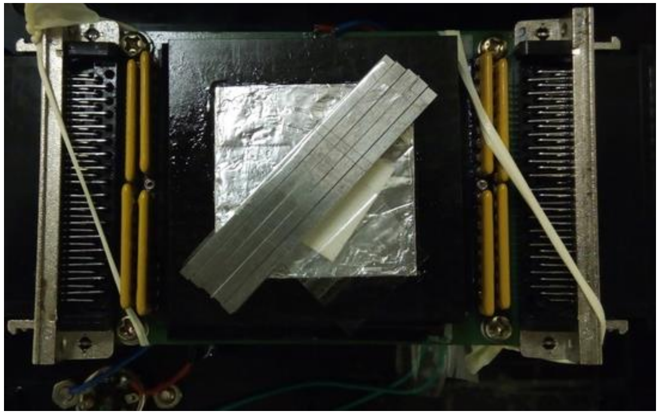

Capillary tube Phantom (Filled with a **^{99m}Tc** source solution):

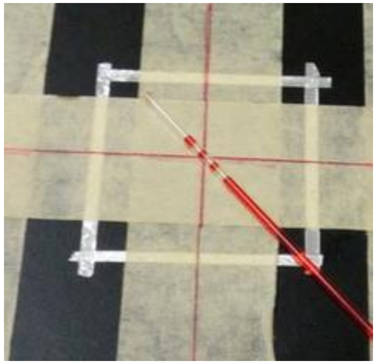

Intrinsic assessment

1 2 9 0 UNIVERSIDADE D COIMBRA

- Results without any scanning calibration, only flood field data used to run the adaptive algorithm (for LRFs)

Spatial resolution:

GAGG prototype: **0.90 mm** FWHM | **LYSO** prototype: **0.72 mm** FWHM

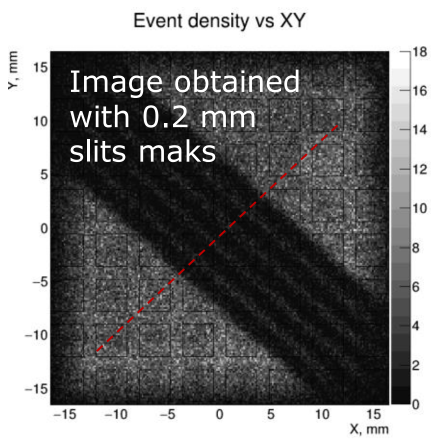

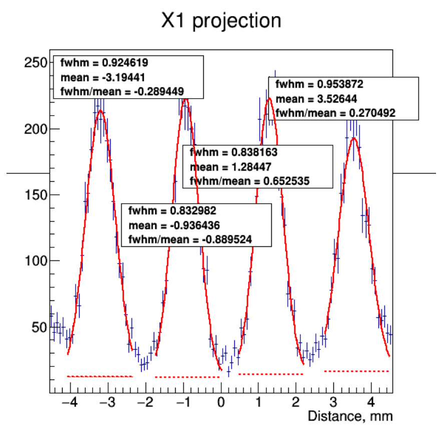

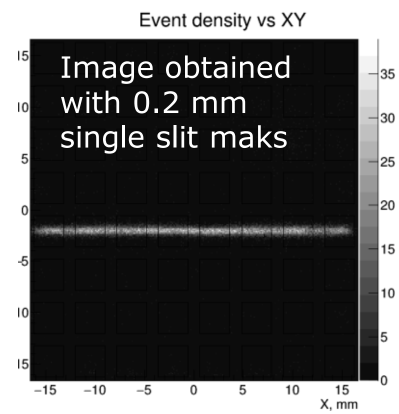

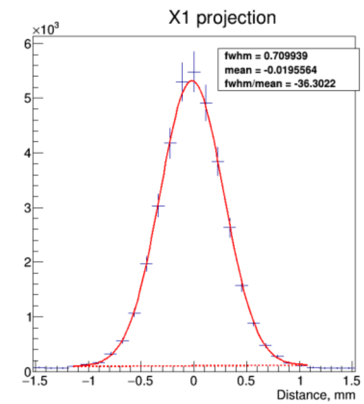

Linearity:

Images obtained with 2 mm parallel bars maks

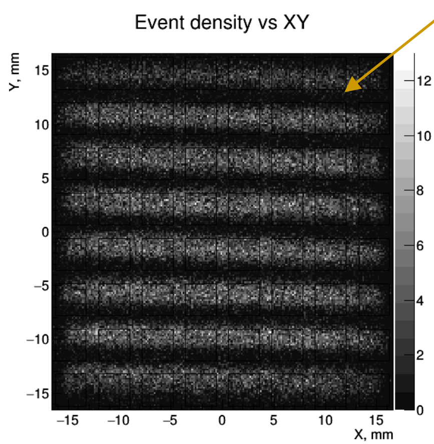

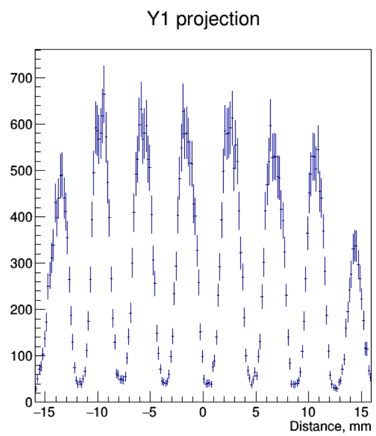

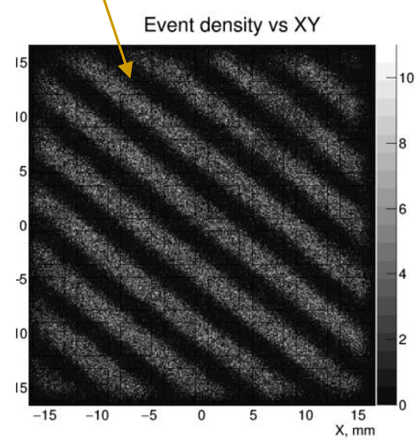

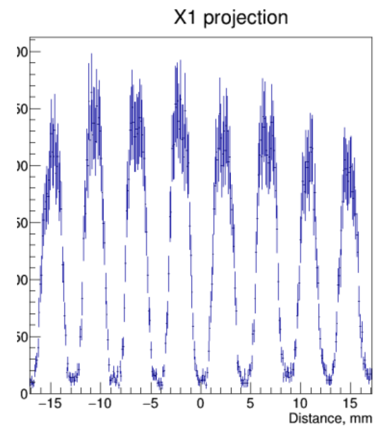

Parallel-hole collimator

(1.5 mm FWHM at 5.8 mm)

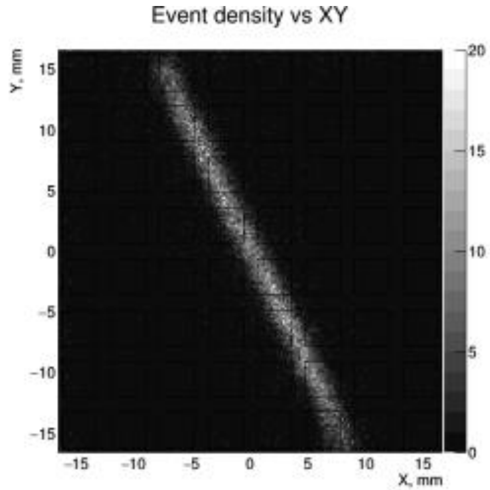

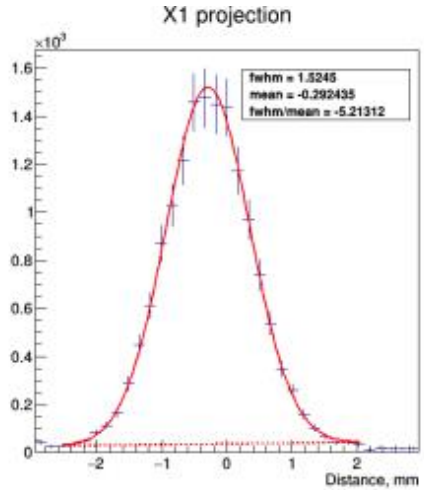

Pinhole collimator

M = 2.24, FWHM = 2.21 mm
(object res. = 0.98 mm FWHM)

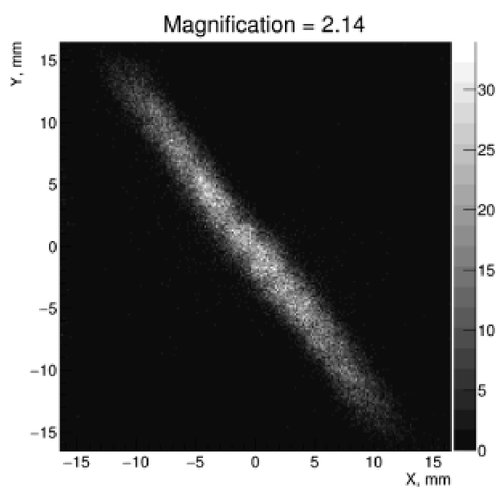

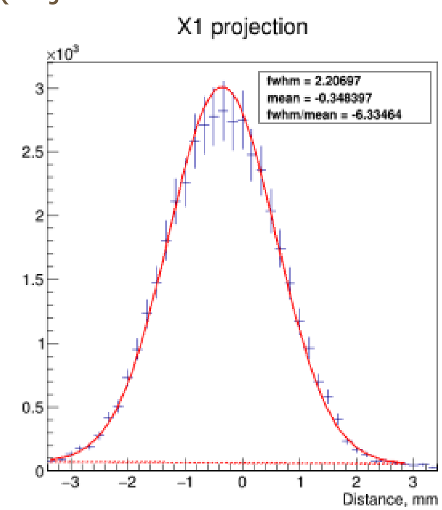

Camera
+
parallel-hole
collimator inside a light tight box

Pinhole collimator

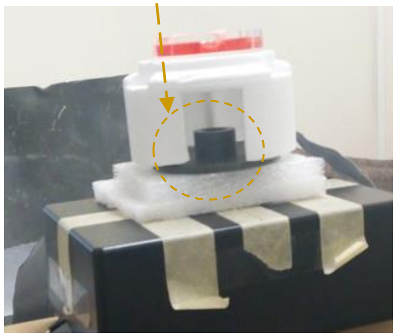

Resolution at the object plane: spatial resolution at the detector plane divide by M.

M: magnification factor

Extrinsic spatial resolution

Extrinsic spatial resolution (cm)

Parallel-hole collimator:

Measured (FWHM):

1.5 mm at 5.8 mm
2.8 mm at 31 mm
3.9 mm at 50 mm
4.4 mm at 60 mm
7 mm at 106 mm

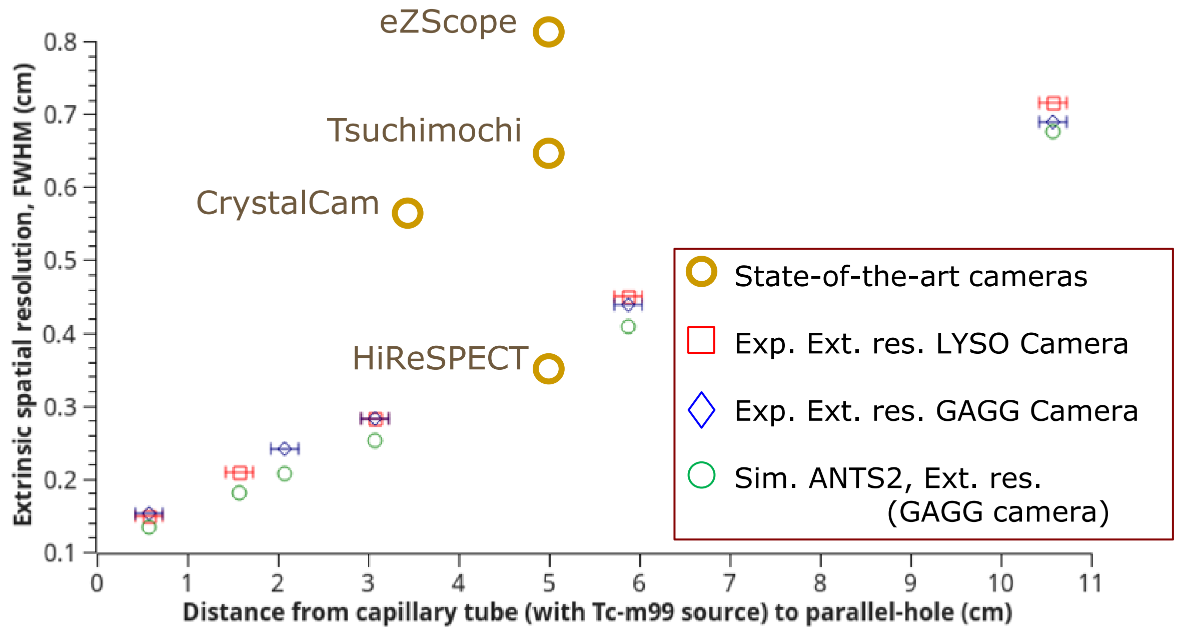

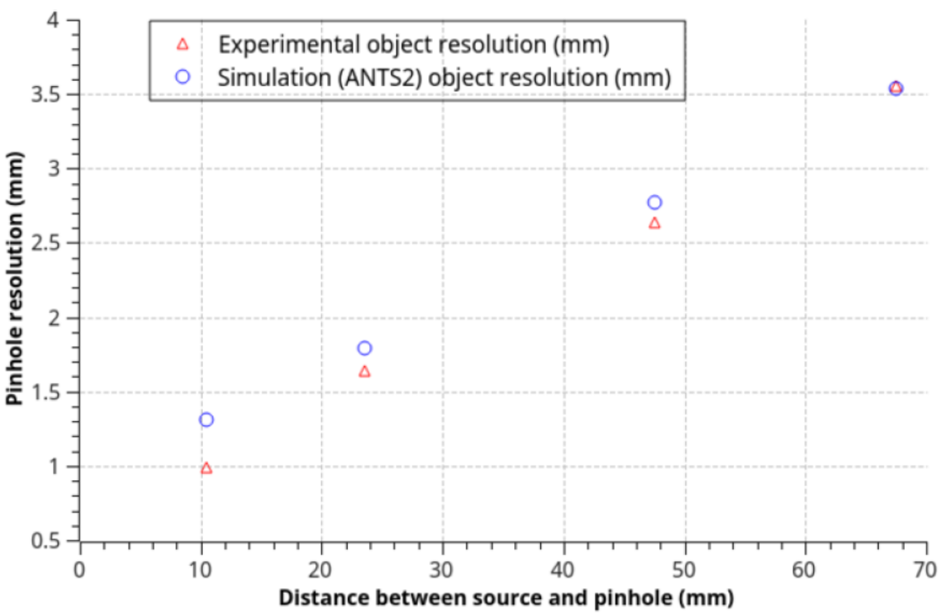

Pinhole collimator:

M	Resolution detector plane (FWHM):	Object res (FWHM):
0.36	1.27 mm	3.53 mm
0.50	1.31 mm	2.62 mm
1.00	**1.64 mm**	**1.64 mm**
2.24	2.21 mm	0.98 mm

PINHOLE COLLIMATOR

PARALLEL-HOLE COLLIMATOR

Brain slice phantom

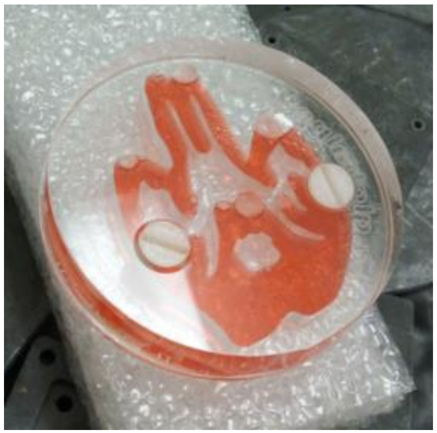

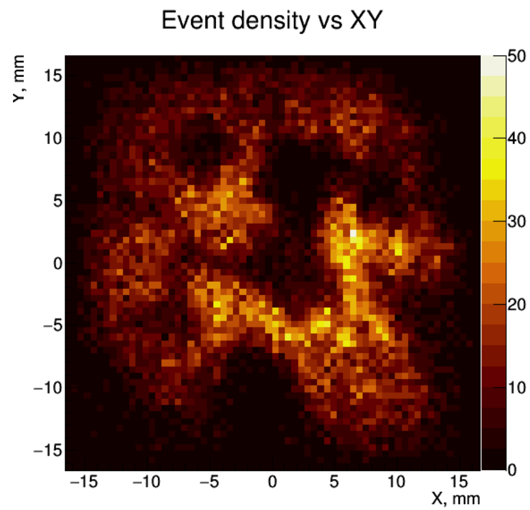

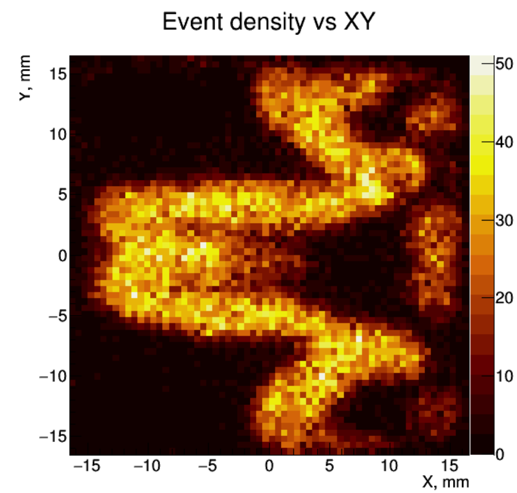

Crossed capillary tubes phantom (parallel-hole collimator)

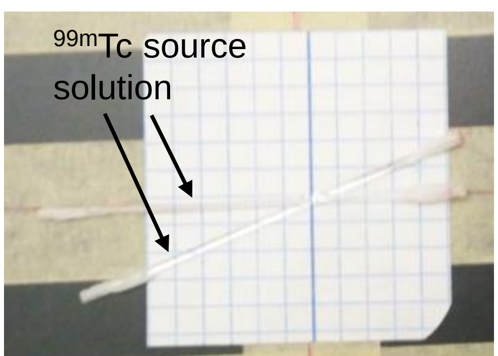

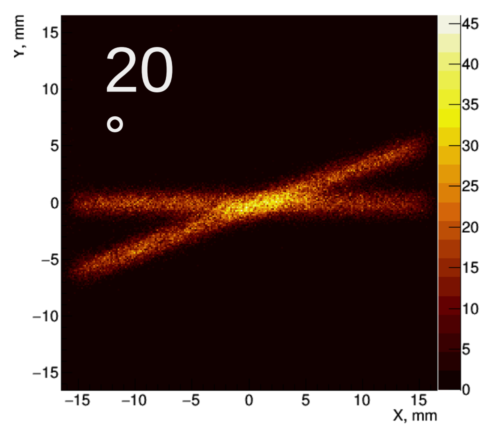

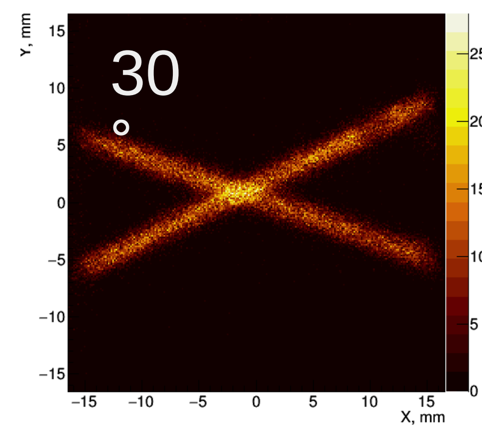

Main results

- The predictive power of the simulation **model** of the camera was successfully validated
- A **prototype** of the compact camera was assembled and was characterized in the hospital (^{99m}Tc source). It was shown that the **requirements are met**
- **Intrinsic spatial resolution** better than 1 mm
- **Extrinsic spatial resolution** (with collimator):

  1.0 mm FWHM (pinhole and 2x magnification)
  3.9 mm FWHM @ 50 mm source - parallel-hole collimator

- **Self-calibration** was confirmed for the new design GAGG camera
- Script **for automatic execution of the interactive procedure** was developed to estimate the camera response model (light response functions)
- **Real-time imaging** was demonstrated
- **Real-time monitoring** of the camera response model, which can trigger an alarm for self-calibration

Nuclear imaging experts from the hospital have confirmed that the developed system can be beneficial for **thyroid nodules functional studies** and for **sentinel lymph node biopsy**

Conclusions: future work

- Perform ***in vivo* imaging of small organs**: clinical test of full-scaled camera (50x50 mm^2) for thyroid imaging at nuclear medicine department of University Hospital of Coimbra

- Evaluate the possibility of apply **self-calibration using the radiation from** the radiotracer already injected into the **patient (method does high degree if uniformity)**

- To build and to test a prototype of a **gamma camera with a larger FOV**, as for large organs (e.g. heart, kidney, lung) the FOV of the developed camera is insufficient

- Integration of the developed camera in a **SPECT device to image the 3D distribution** of the radiotracer inside the body

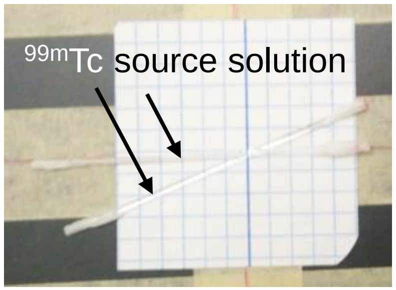

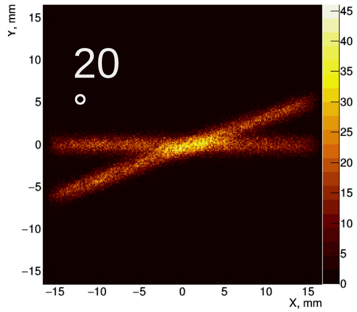

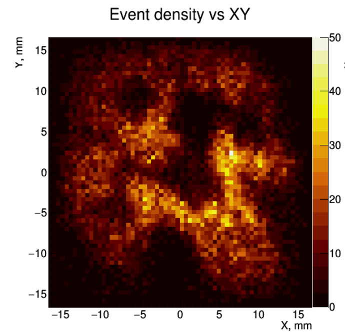

Pinhole collimator

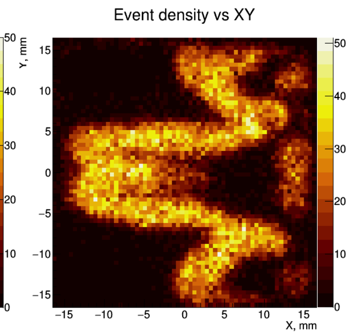

Parallel-hole collimator

Thank you very much for your attention

CAFÉ COM FÍSICA AUDIENCE

Special thanks to Doctor Vladimir Solovov and Doctor Andrey Morozov (colleagues in the Gamma Cameras Group) and Doctor Vitaly Tchepel

End of presentation

DISCUSSION OPENED TO COMMENTS AND QUESTIONS

EXTRA slides below

IF FURTHER CLARIFICATIONS ARE REQUIRED

Camera design: optimization of lightguide thickness

DEPTH OF INTERACTION ANALYSIS

Depth of interaction (DoI) in a 3 mm thick GAGG scintillator

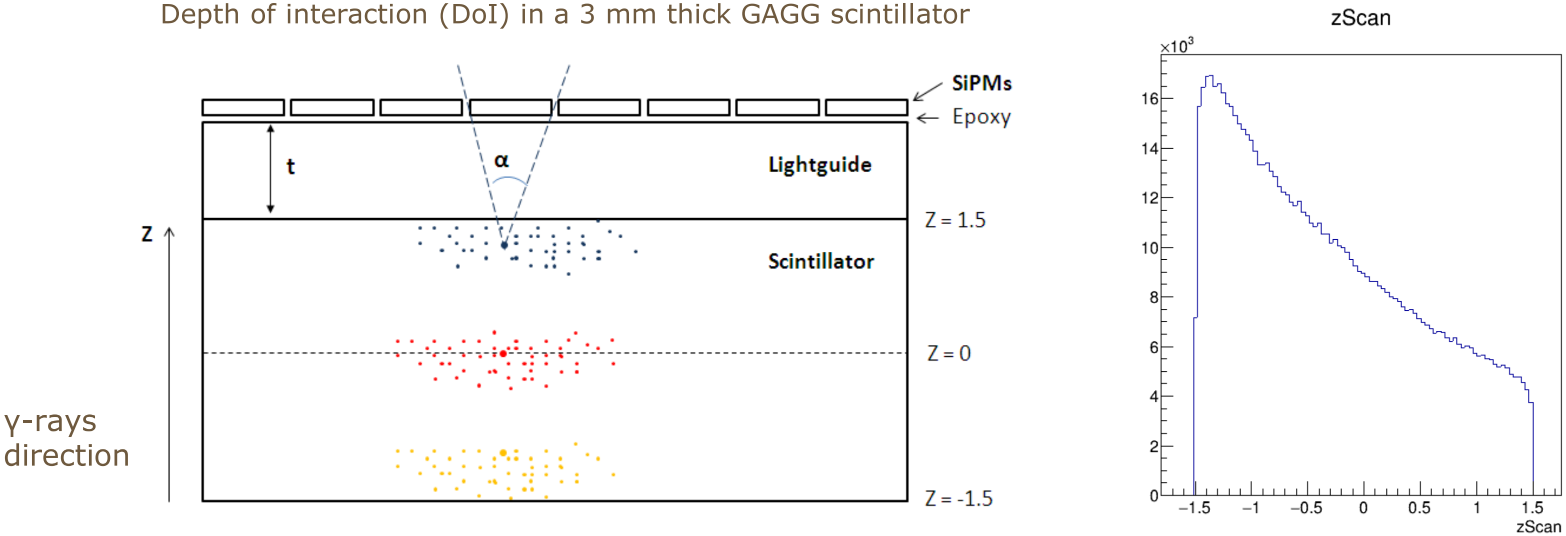

Histogram of DoI position

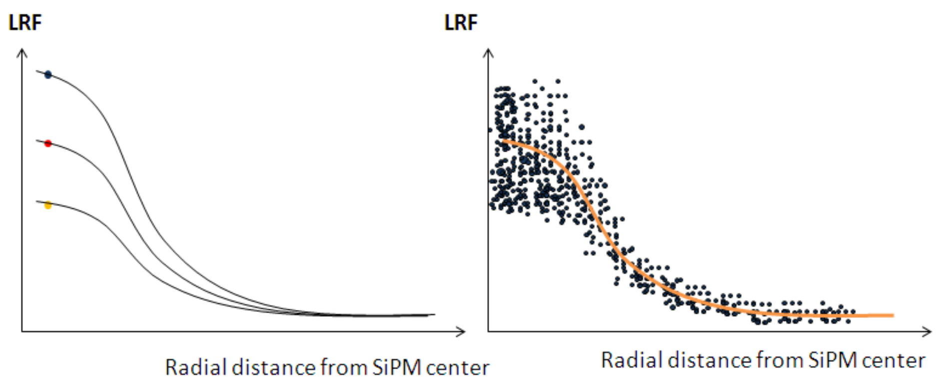

Illustration of the light response function of a photosensor (camera response model)

Optimization of lightguide thickness

SIMULATION STUDY (3 mm thick GAGG crystal and lightguide thickness from 0.3 mm to 1.5 mm)

SIMULATION: emission of **one million 140 keV γ-rays** uniformly distributed over that area

The XY density plot of the reconstructed positions using the LRFs estimated with all events but filtering out the scintillation positions out of **(a)** the central, **(b)** bottom, **(c)** top regions, respectively. **(d)** All events included

The analysis on the reconstruction performance was only performed for a quarter of the camera area (16.6 × 16.6 mm 2 in the upper-right corner).

Density plot of reconstructed positions (**1.0 mm thick lightguide**)

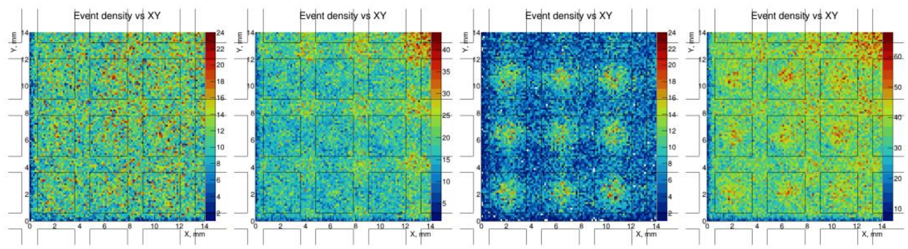

(a) (b) (c) (d)

Figure 3.32: Density plot of reconstructed positions (3 mm thick GAGG and 1.0 mm thick lightguide). a: Using only events from the central region of the scintillator; b: Using only events from the bottom region of the scintillator; b: Using only events from the top region of the scintillator; d: Using all events.

XY density plot of the average differences between the X coordinate of the reconstructed and true positions (**0.3 mm thick lighguide**)

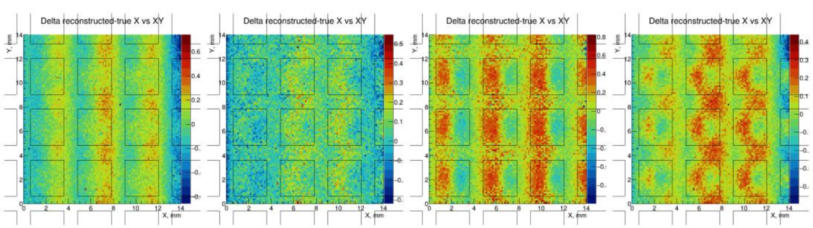

(a) (b) (c) (d)

Figure 3.33: XY density plot of the average differences between the X coordinate of the reconstructed and true positions (3 mm thick GAGG and 0.3 mm thick lighguide). a: Using only events from the bottom region of the scintillator; b: Using only events from the central region of the scintillator; c: Using only events from the top region of the scintillator; d: Using all event.

Density plot of reconstructed positions (**0.3 mm thick lightguide**)

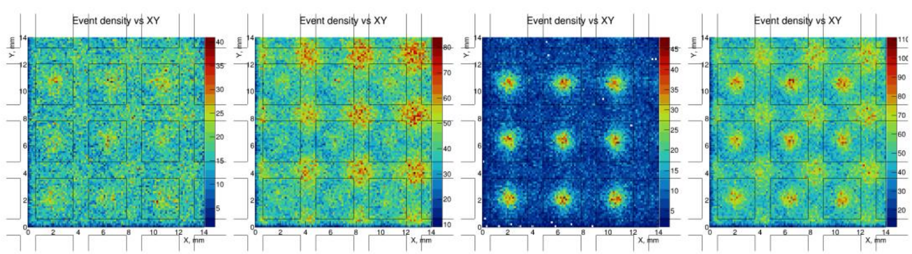

(a) (b) (c) (d)

Figure 3.34: Density plot of reconstructed positions (3 mm thick GAGG and 0.3 mm thick lightguide). a: Using only events from the central region of the scintillator; b: Using only events from the bottom region of the scintillator; c: Using only events from the top region of the scintillator; d: Using all events.

Optimization of lightguide thickness

SIMULATION STUDY

XY Density plot of reconstructed positions of a 99m-Tc source projection through a diagonal slit

0.8 mm

0.3 mm

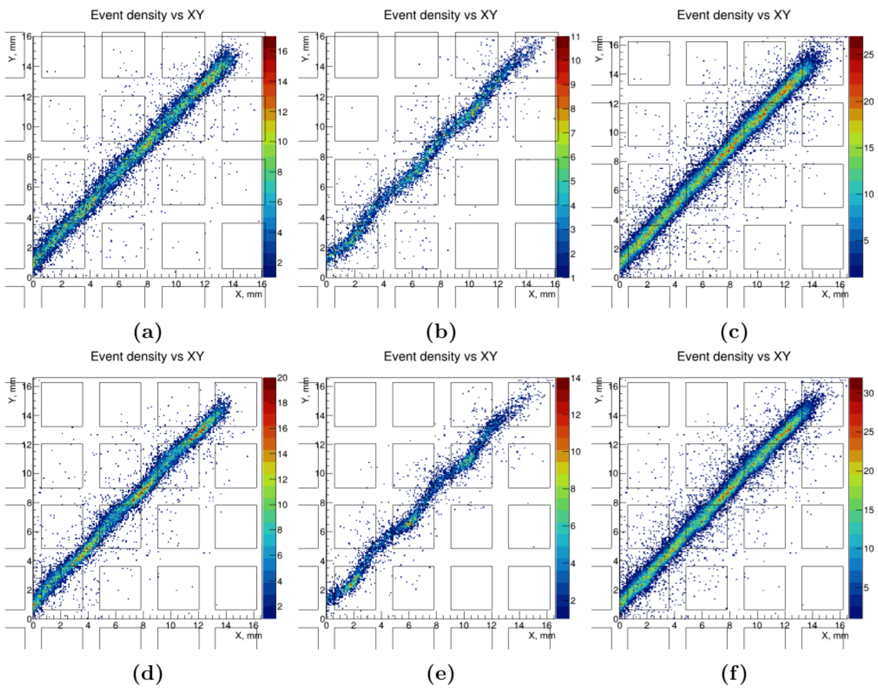

Figure 3.35: XY Density plot of reconstructed positions of a ^{99m}Tc source projection through a diagonal slit (3 mm thick GAGG). a, b and c: 0.8 mm thick lightguide; d, e and f: 0.3 mm thick lightguide; a and d: Using only events from the bottom region of the scintillator; b and e: Using only events from the top region of the scintillator; c and f: Using all events.

Optimal lightguide thickness: 0.8 mm – 1.0 mm

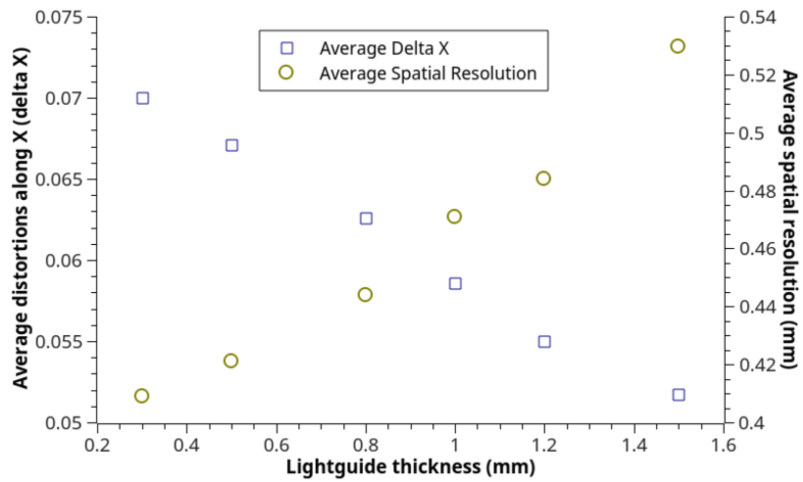

Optimization of coupling between camera elements

Using commercially available optical adhesives

Single optical grease
(low refractive index, n = 1.465)

Teflon	n= 1.37
Optical grease	n = 1.465
GAGG:Ce	n = 1.93
Optical grease	n = 1.465
Lightguide	n = 1.51
Optical grease	n = 1.465
SiPM epoxy	n = 1.47

Three optical adhesives
(high refractive index)

Teflon	n= 1.37
Optical adhesive	n = 1.66
GAGG:Ce	n = 1.93
Optical adhesive	n = 1.73
Lightguide	n = 1.73
Optical adhesive	n = 1.57
SiPM epoxy	n = 1.47

Ex.of iterative method for compact camera

- Diagonal line of pencil beam sources

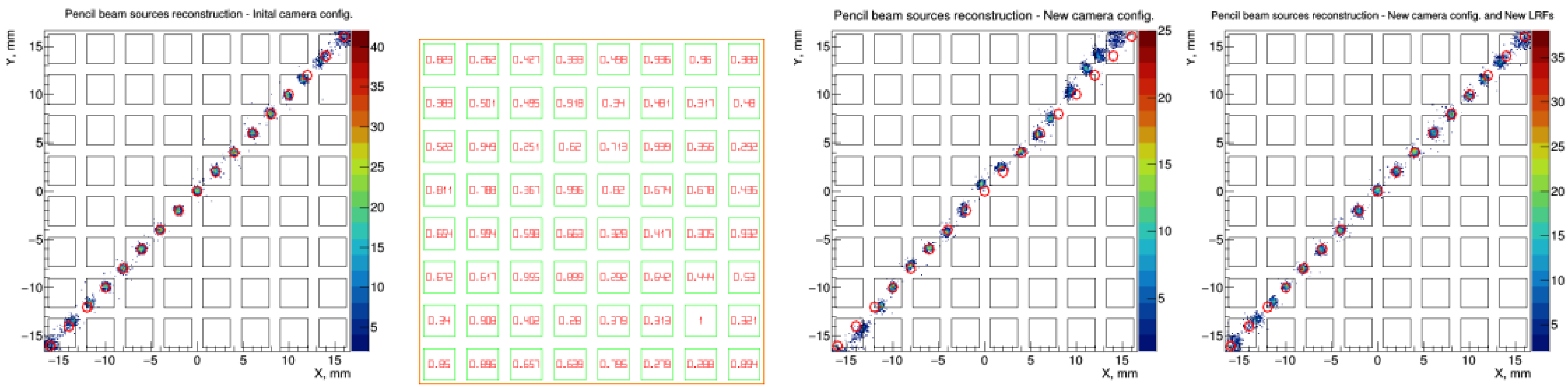

(a) (b) (c) (d)

Figure 5.7: Example of the automatic algorithm capacity to accurately estimate LRFs. a: XY density plot of the reconstructed pencil beam sources using LRF_1 (initial camera configuration). The read circles are the true source positions. b: Map with the relative gains randomly set to each SiPM (active areas are delimited by a thin green lines). c: XY density plot of the reconstructed pencil beam sources using LRF_1 (changed camera configuration). Strong distortions are apparent. d: XY density plot of the reconstructed pencil beam sources using LRF_{new} (changed camera configuration).

Characterisation of the difference

BETWEEN THE EXPECTED AND OBSERVED VALUES

- Maximum Likelihood

Probability density function

$$W(x,y,e) = \prod_{i}^{\# PMTs} P_i \ (A_i, a_i(x,y,e))$$

- Least squares

$$\chi^2(x,y,e) = \sum_{i}^{\# PMTs} \left(A_i - a_i(x,y,e)\right)^2$$

Optimization

Process of finding the position which gives the **best match between the vector of measured signals and that with the predicted signals**.

Simplest approach (and slowest): Brute force
Alternatives: **Contracting grids**, migrad and simplex

→ The **"contracting grids" technique**, which is faster than brute force because it does not perform high resolution search over the entire parameter space. A grid is defined around a certain region and the search is performed. Depending on the required precision, a new, finer grid is defined around the optimal position and the search starts again. The new optimal position is calculated and this process can iterate, decreasing the step between the grid nodes until the finest grid, which is usually smaller than the spatial resolution.

The vacancy created by the electron ejected from the atom will be filled with other electron from an upper shell, reestablishing the atom lowest energy state. This **relaxation** can occur either through **fluorescence**, with the emission of an X-ray, or through a nonradioactive transition, with the emission of an Auger electron.
These two secondary effects of photoelectric absorption have complementary probabilities

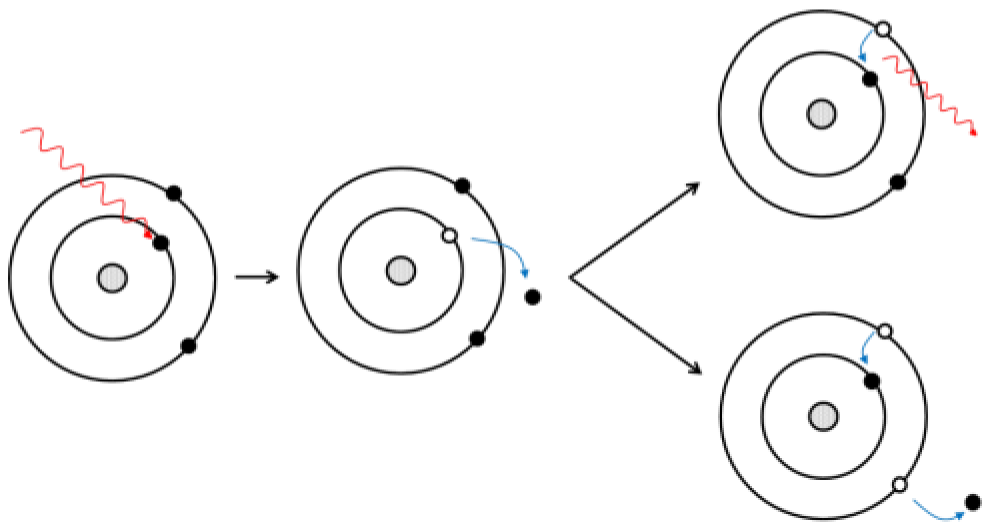

Figure 2.2: Photoelectric absorption and secondary effect representation. One γ-ray (red arrow on the left) interacts with an atom and a photoelectron is ejected (blue arrow on the left) leaving a vacancy. Fluorescence or a emission of an Auger electron can occur with complementary probabilities. The image was copied from [14].

Using **CrystalCam** hand-held camera:

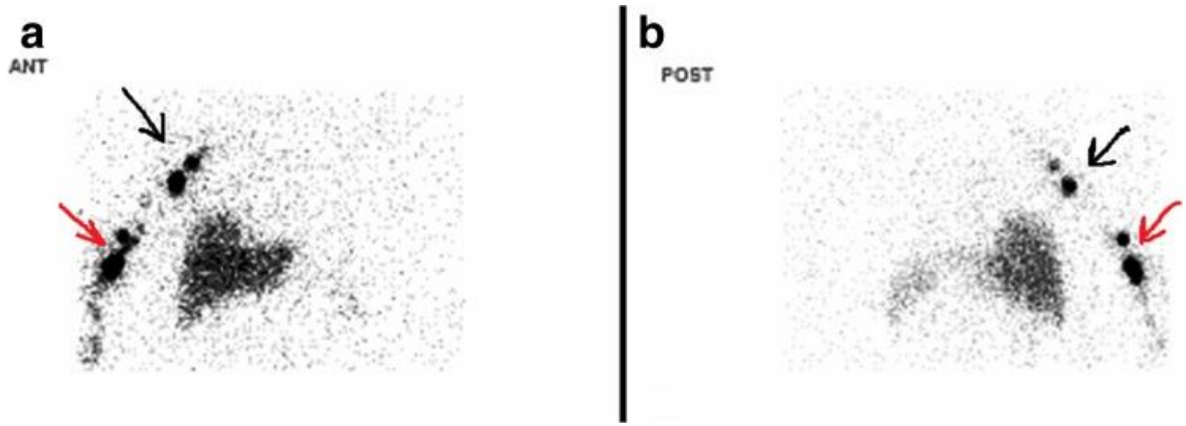

Anterior (**a**) and posterior (**b**) static images from the thoracal region were taken by dual-headed gamma camera. Axillar (*black arrow*) and epitrochlear (*red arrow*) lymphatic drainage was seen on the right upper extremity

The Utility of Intraoperative Handheld Gamma Camera for Detection of Sentinel Lymph Nodes in Melanoma
Elgin Ozkan and Aydan Eroglu

Nucl Med Mol Imaging. 2015 Dec; 49(4): 318–320.
doi: 10.1007/s13139-015-0341-5

Geant4 vs ANTS2 energy deposition

SIMULATIONS | G4ANTS INTERFACE SOFTWARE

ANTS2

Send to Geant4 based application:

- Detector geometry (GDML format)
- Materials chemical composition
- Name of scintillator component
- Number of primary gamma-rays to simulate
- File with particle information:
  - Particle ID
  - Energy
  - Time
  - Position (x, y, z)
  - Direction vector (Vx, Vy, Vz)

- Generate optical photons (based on the recieved positions, energies and the scintillator light-yield)
- Simulate tracking of optical photons

Geant4

Simulate energy deposition

For each primary gamma-ray sends back to ANTS2, for each deposition node:

- Deposited energy
- Deposition time
- Position of the energy deposition

Geant4 vs ANTS2 simulation of energy deposition

SPATIAL RESOLUTION RESULTS COMPARISON (LYSO crystal)

Geant4

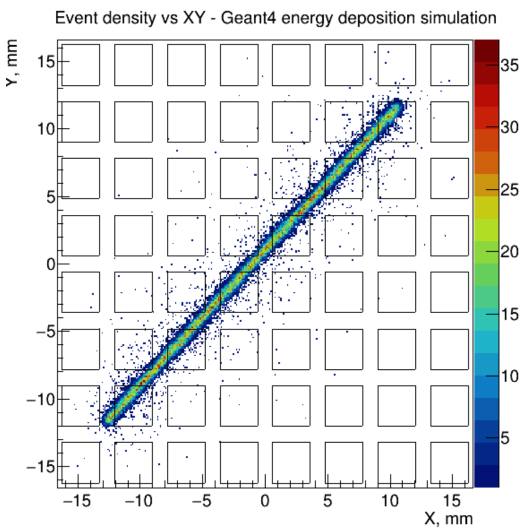

0.64 mm FWHM

ANTS2

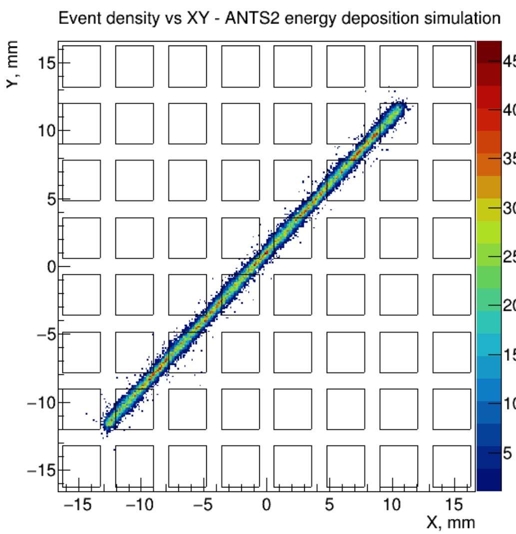

0.52 mm FWHM

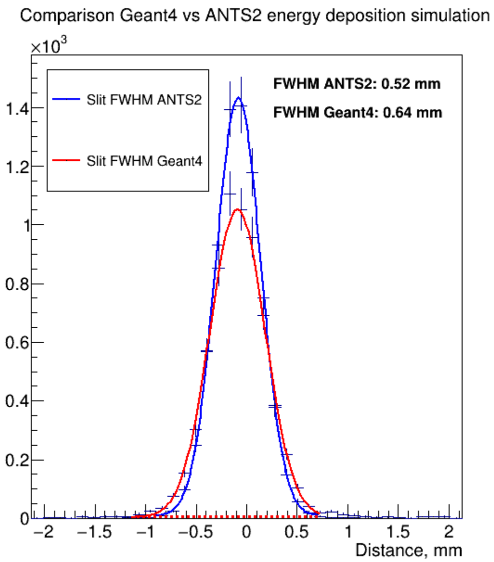

This difference of 23% is attributed mostly to K-shell fluorescence of Lu (53-63 keV), which is only simulated in Geant4.

Geant4 vs ANTS2 simulation of energy deposition

ENERGY RESOLUTION RESULTS COMPARISON (LYSO crystal)

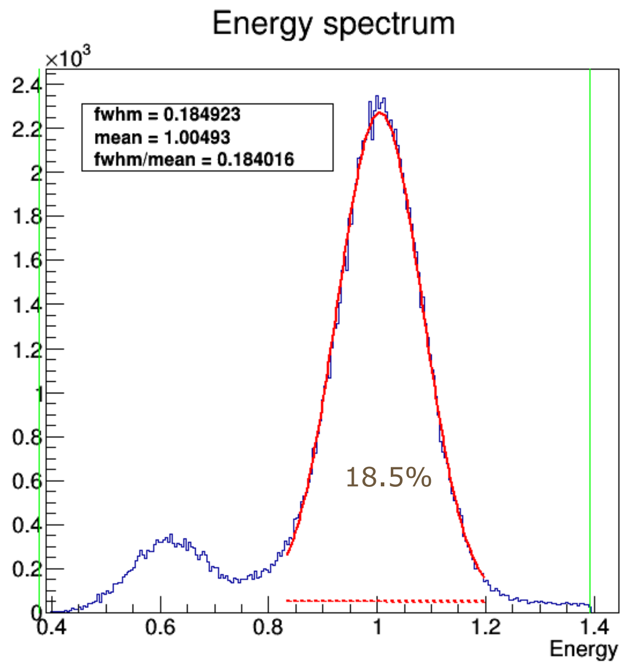

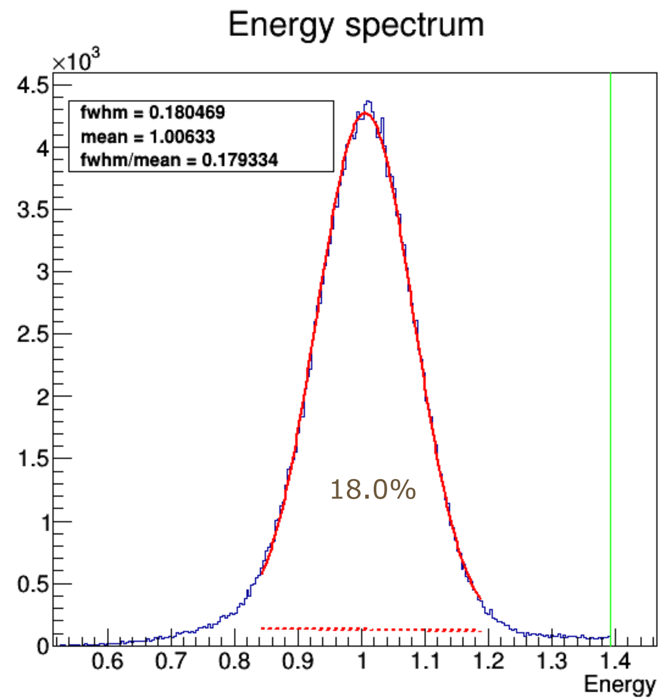

Readout and acquisition system

TRB3 (GSI) BASED READOUT FOR 64 CHANNELS

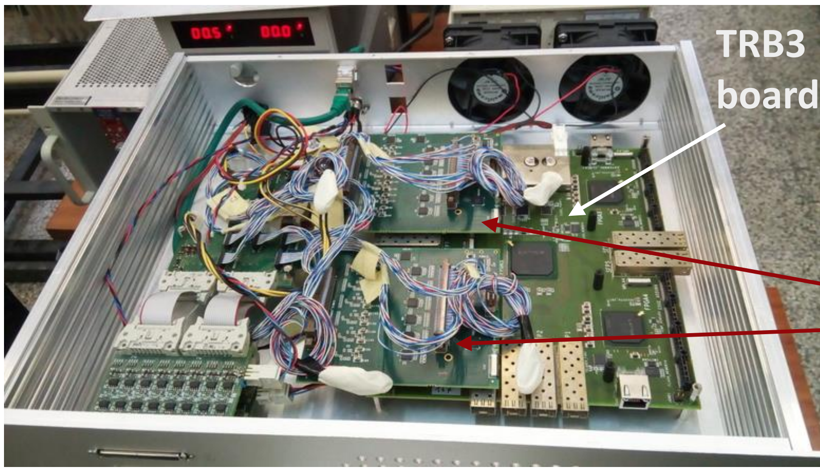

Constructed and programmed with help of Alberto Blanco and João Saraiva (LIP Coimbra)

Odroid-C2 mini-computer:

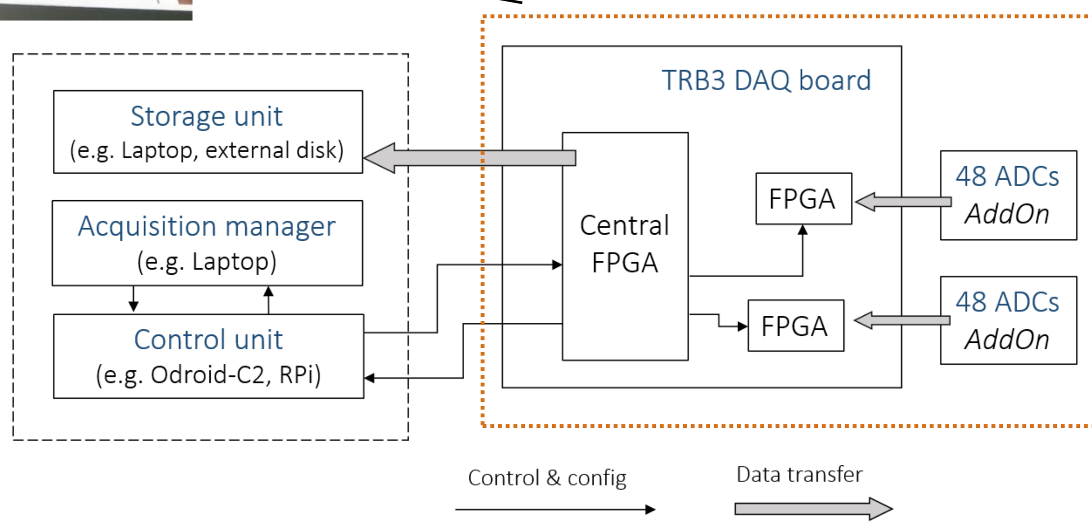

Data acquisition system performance

TRANSFER RATE AND ACQUISITION RATE

Transfer rate

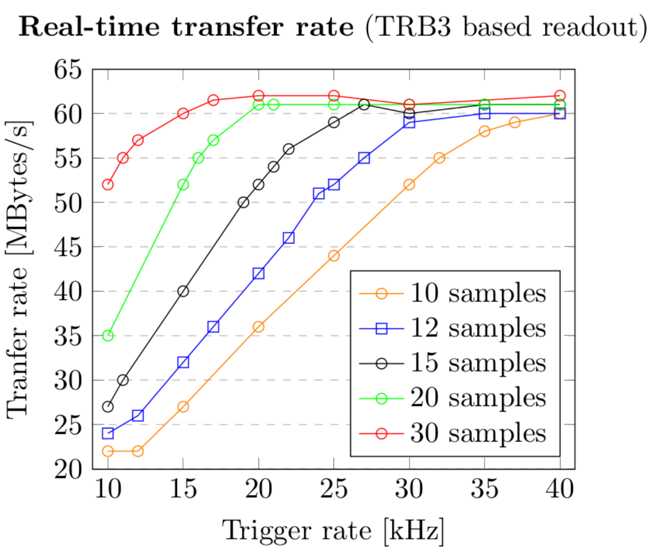

Acquisition rate *vs* # of waveform samples

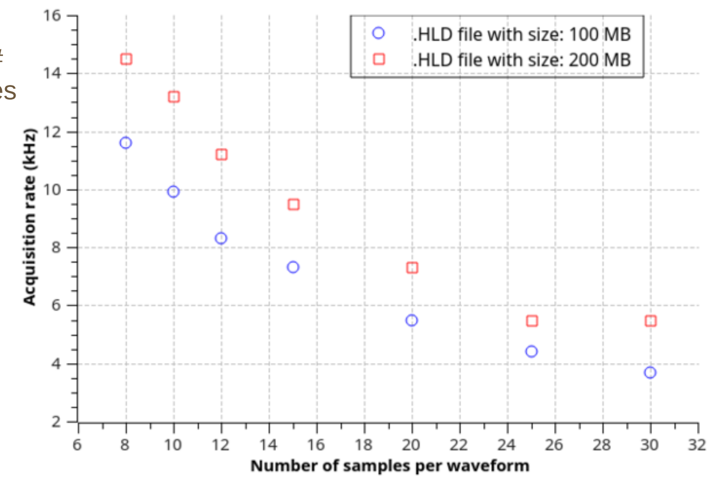

Acquisition rate *vs* size

of data files (.HLD files)

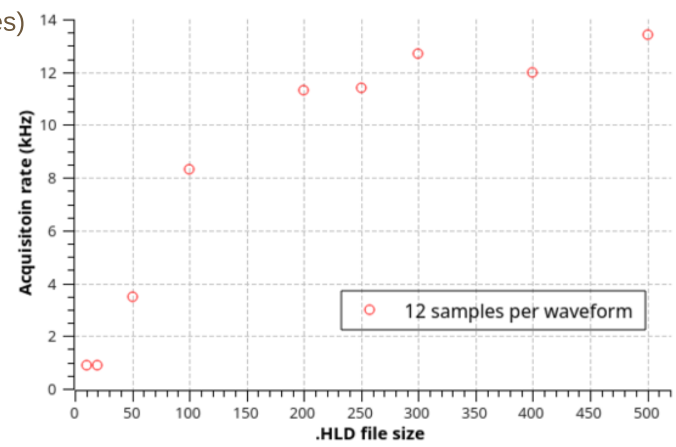

Reconstruction time *vs* # of used **processor threads**

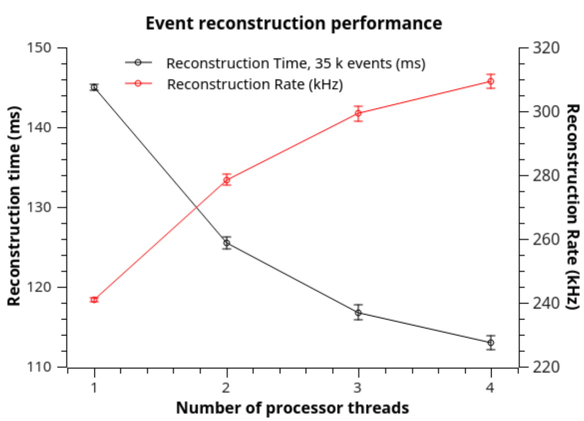

Masks and phantoms

Source position

Masks:

Parallel bars 2 mm wide

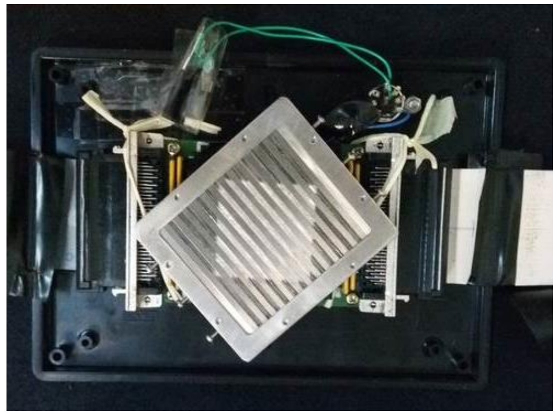

Four parallel 0.2 mm slits

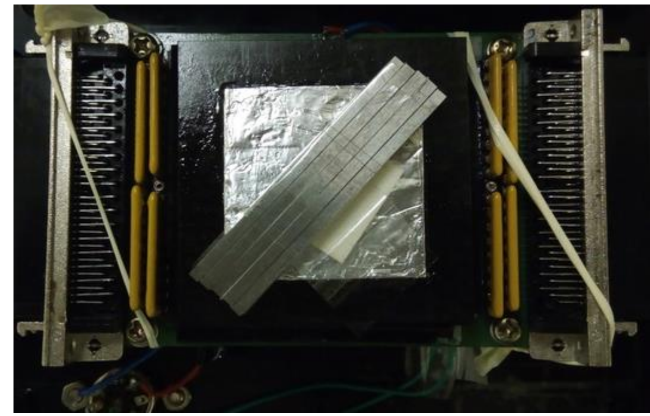

Phantoms (Filled with a **^{99m}Tc** source solution):

Capillary tubes

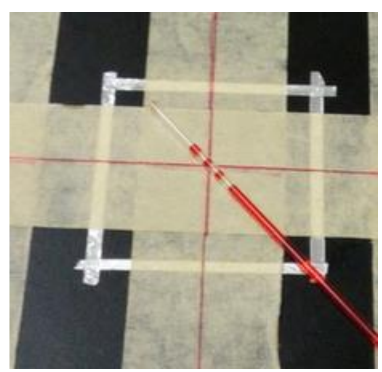

"Brain slice" phantom

Real-time imaging
SNAPSHOTS

ANTS2 reconstruction and visualization in real-time

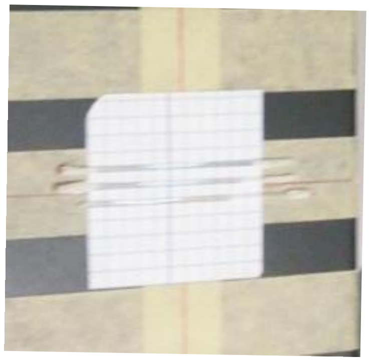
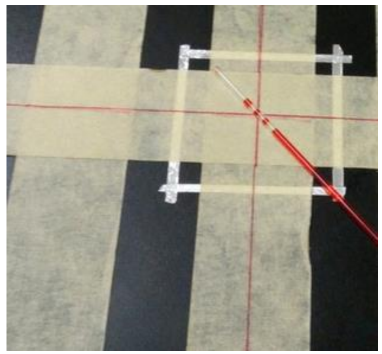


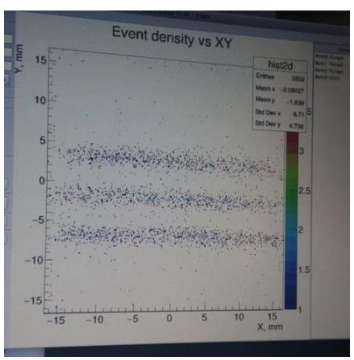

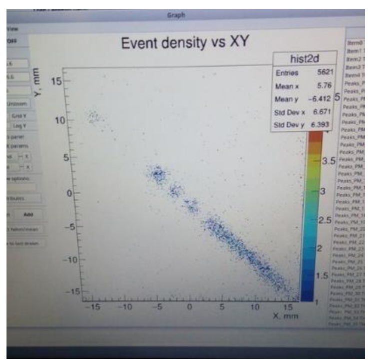

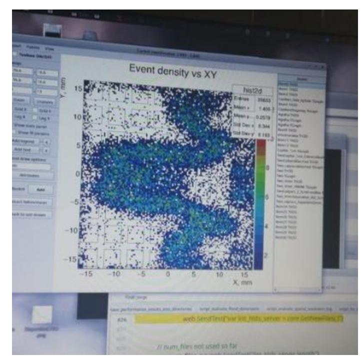

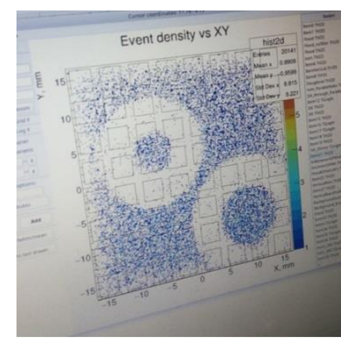

Prototype details

photographs

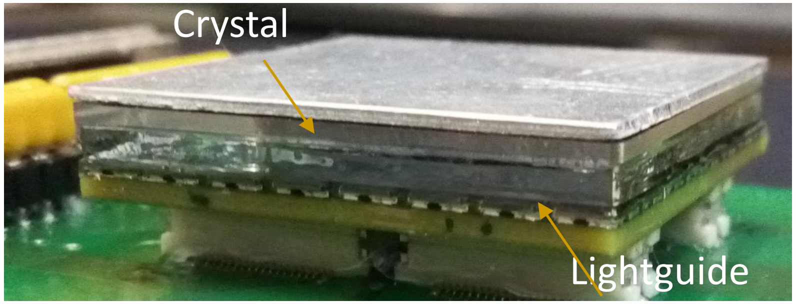

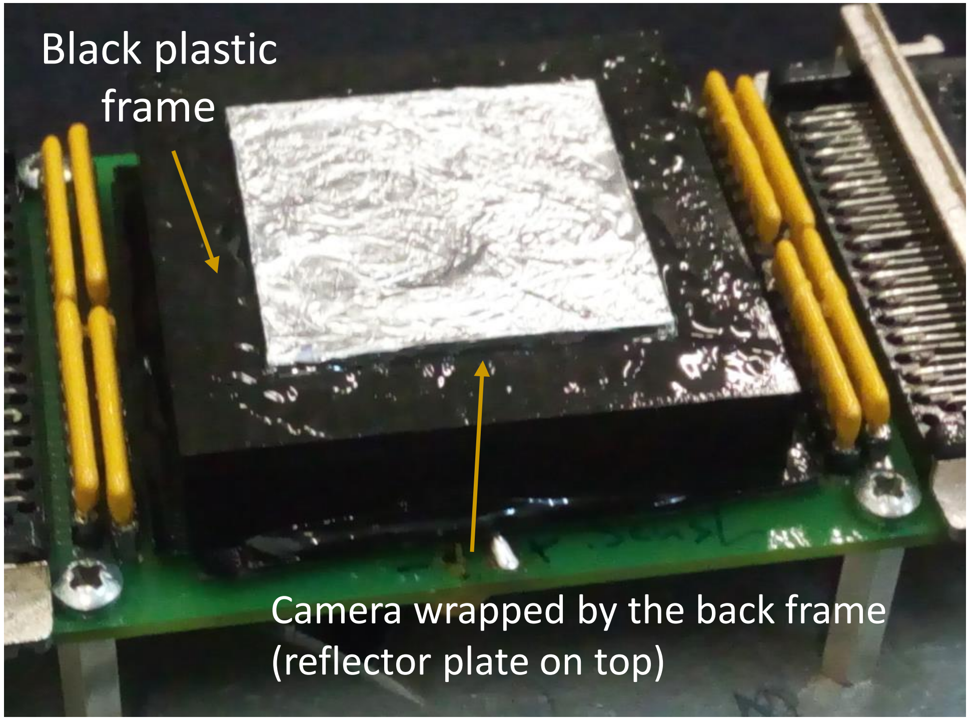

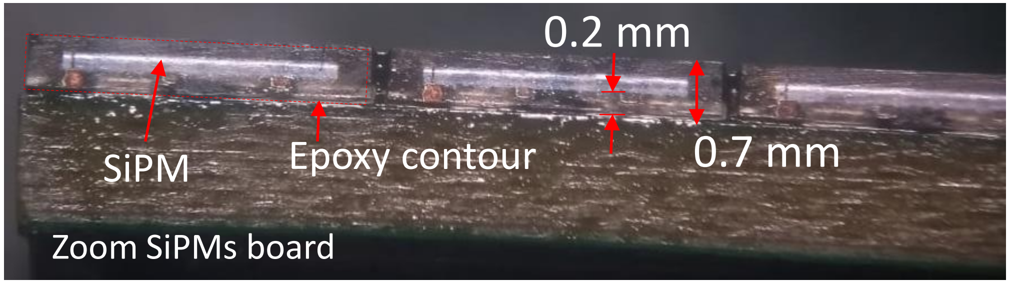

Light response functions

One LRF for each photosensor

- The model is a set of light response functions (LRFs)

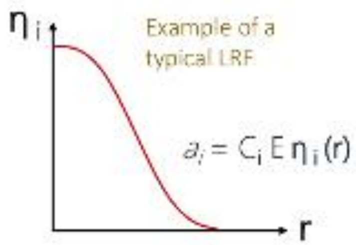

LRF for one photosensor in a 30 x 30 mm square camera

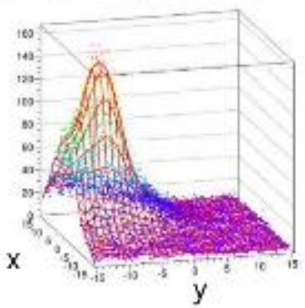

LRF for a clinical gamma camera Ø500 mm

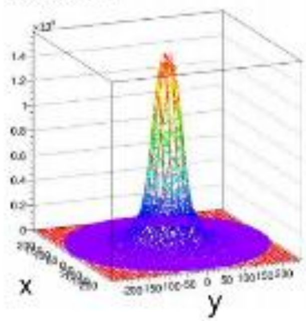

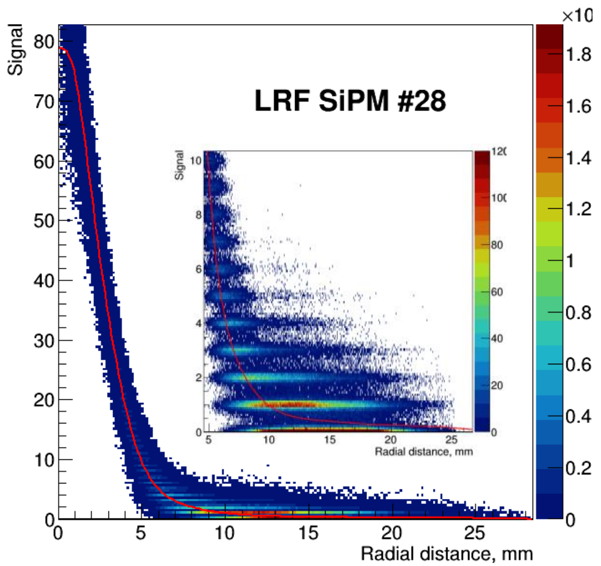

Radial distance from the center of the photosensor to the light emission position

Scintillator materials
EXAMPLES OF INORGANIC CRYSTALS

Material	Density (g/cm^3)	λ_{max} (nm)	Refractive index	τ (ns)	Light yield (Ph/MeV)
NaI(Tl)	3.67	415	1.85	230	38000
CsI(Tl)	4.51	540	1.80	800	60000
$Bi_4Ge_3O_{12}$	7.13	480	2.15	300	8200
BaF_2	4.89	220, 310	1.56	0.6, 630	1500, 9500
CeF_3	6.16	340	1.68	27	4400
Lu_2SiO_5(Ce)	7.4	420	1.82	47	25000
$LaBr_3$(Ce)	3.79	350	1.9	27	49000